Coarse-Grained Model-Assisted Design of Optimized Polymer Prodrug Nanoparticles: A Combined Theoretical and Experimental Study

Ping Gao,[†,‡] Tâp Ha-Duong,[*,†] and Julien Nicolas[*,‡]

†*Université Paris-Saclay, CNRS, BioCIS, Orsay, 91400, France*

‡ *Université Paris-Saclay, CNRS, Institut Galien Paris-Saclay, Orsay, 91400, France*

E-mail: tap.ha-duong@universite-paris-saclay.fr; julien.nicolas@universite-paris-saclay.fr

Abstract

To achieve efficient drug release from polymer prodrug nanoparticles, the drug-polymer linker must be accessible for cleavage to release the drug, which can occur under certain physiological conditions (e.g., presence of specific enzymes). Supramolecular organization of polymer prodrug nanoparticles is crucial as it greatly affects the location of the linker, its surface exposure/solvation and thus its cleavage to release the drug. Since experimental access to this data is not straightforward, a new methodology is critically needed to access this information and to accelerate the development of more effective polymer prodrug nanoparticles, and replace the time-consuming and resource-intensive traditional trial-and-error strategy. In this context, we developed a coarse-grained model-assisted design of optimized polymer prodrug nanoparticles. By choosing the solvent accessible surface area as the critical parameter for predicting drug release and hence cytotoxicity of polymer prodrug nanoparticles, we developed an optimized polymer-drug linker with enhanced hydrophilicity and solvation. Our hypothesis was then experimentally validated by the synthesis of the corresponding polymer prodrugs based on two different drugs (gemcitabine and paclitaxel), which demonstrated greater performances in terms of drug release and cytotoxicity on two cancer cell lines. Interestingly, our methodology can be easily applied to other polymer prodrug structures, which would contribute to the development of more efficient drug delivery systems.

Introduction

Prodrugs are molecules which are metabolized by living organisms into pharmacologically active drugs. Prodrugs are precursors of drugs and are primarily used to improve the bioavailability of drugs with unfavorable pharmacokinetics properties.[1-5] They can also be used to improve drug selectivity to their intended target, thus reducing their undesirable side effects.[6-10] When this concept is applied to polymers (i.e., by coupling drugs to polymers),[11] the resulting polymer prodrugs can also take benefit from the polymer properties. They can for instance self-assemble into nanoparticles to efficiently protect drugs from early degradation, prolong their systemic circulation time, and deliver their payloads in diseased tissues by enhanced permeation and retention effect and/or via specific cleavage of the polymer-drug linker.[12-17] The linker plays an essential role in polymer prodrug systems as not only does it prevent the uncontrolled "burst" release of the drug often experienced with non-covalent drug-loaded polymer nanocarriers, but it also controls the drug release kinetics and therefore the rate of prodrug metabolization into active drug, and ultimately therapeutic effect. To control the drug release from polymer prodrug nanoparticles, the polymer-drug covalent bond must be cleaved under specific conditions. This can be achieved by using pH-sensitive labile linkers,[18] such as imines,[19] amides,[20] or hydrazones,[21] which would be hydrolyzed only in acidic environment of diseased tissues. Alternatively, over-expression of specific enzymes in pathological cells, such as esterases or cathepsins, is another endogenous stimulus which can be used to cleave specific functional groups, such as ester or amide bonds.[22-26]

Polymer prodrug nanoparticles are essentially obtained by formulation of the presynthesized polymer prodrugs, for instance by nanoprecipitation (also called solvent displacement/exchange method[27]). Depending on the physico-chemical properties of the polymer prodrugs (e.g., water solubility of the drug and the polymer, position of the drug on the polymer chain), they will adopt a certain spatial organization during nanoparticle formation, which will have a significant impact on the localization of the drugs and, consequently, the linkers. This information is crucial because linkers embedded in the core of nanoparticles will not be easily accessible to enzymes or even solvated for hydrolytic cleavage, unlike linkers exposed at (or near) the surface. Unfortunately, experimental access to this information cannot be achieved by using routine colloids characterization techniques (e.g., dynamic light scattering, (cryogenic) transmission electron microscopy, etc.). Furthermore, while standard surface characterization techniques require dry samples, which

destructure nanoparticle morphology with low glass transition temperature (T_g) polymers, small angle scattering techniques are cumbersome experiments and not always relevant for quantifying the surface composition of nanoparticles.

This is unfortunate because such precise and quantitative information would be valuable to effectively guide the development of new polymer prodrug nanoparticles. This explains, at least in part, why the evaluation of new drug delivery systems is almost exclusively based on the traditional trial-and-error strategy, which relies on synthesizing new structures and evaluating them *in vitro*/*in vivo*. However, this approach is time-consuming, costly and generates significant waste which is unsustainable. To circumvent these limitations, simulation of the supramolecular organization of polymer prodrugs may provide crucial atomic-scale information to predict and adapt the localization of key components (e.g., drugs, linkers) to accelerate the design of more potent drug delivery systems with minimal cost and resources.[28]

Interestingly, coarse-grained modeling allows for simulations on longer time scales (2-3 orders of magnitude) and at a much lower computational cost than all-atom simulations, which is well suited for studies of supramolecular organization of macromolecules.[29] Among the different models, MARTINI force fields, which were initially developed for lipid-based systems, can now be used for a broad range of supramolecular nanostructures,[28,30] including those based on polymers[31,32] and short peptides.[33,34] In this context, we have recently developed a MARTINI-based coarse-grained model to better understand the supramolecular organization of polymer prodrug nanoparticles based on gemcitabine-polyisoprene (Gem-PI) and paclitaxel-polyisoprene (Ptx-PI),[35] which have previously shown promising results for anticancer therapy.[36,37] In particular, we found that the nature of the polymer-drug linkage significantly influences its localization within the nanoassembly and thus its solvation, which could greatly influence the drug release and therefore the therapeutic effect.

However, whether this model can be used to predict, and even optimize, the anticancer efficacy of polymer prodrug nanoparticles remains a critical question that could make this modeling approach of immense interest in drug delivery if it turns out to be the case. Herein, we report on the coarse-grained model-assisted design of an optimized polymer-drug linker with enhanced hydrophilicity and solvation to: (i) avoid the tedious trial-and-error strategy and (ii) produce more effective polymer prodrug nanoparticles than those experimentally obtained so far (Figure 1). We demonstrated the reliability and the versatility of this modeling

approach by its experimental validation on polymer prodrugs based on two different drugs in terms of drug release and cytotoxicity on two different cancer cell lines.

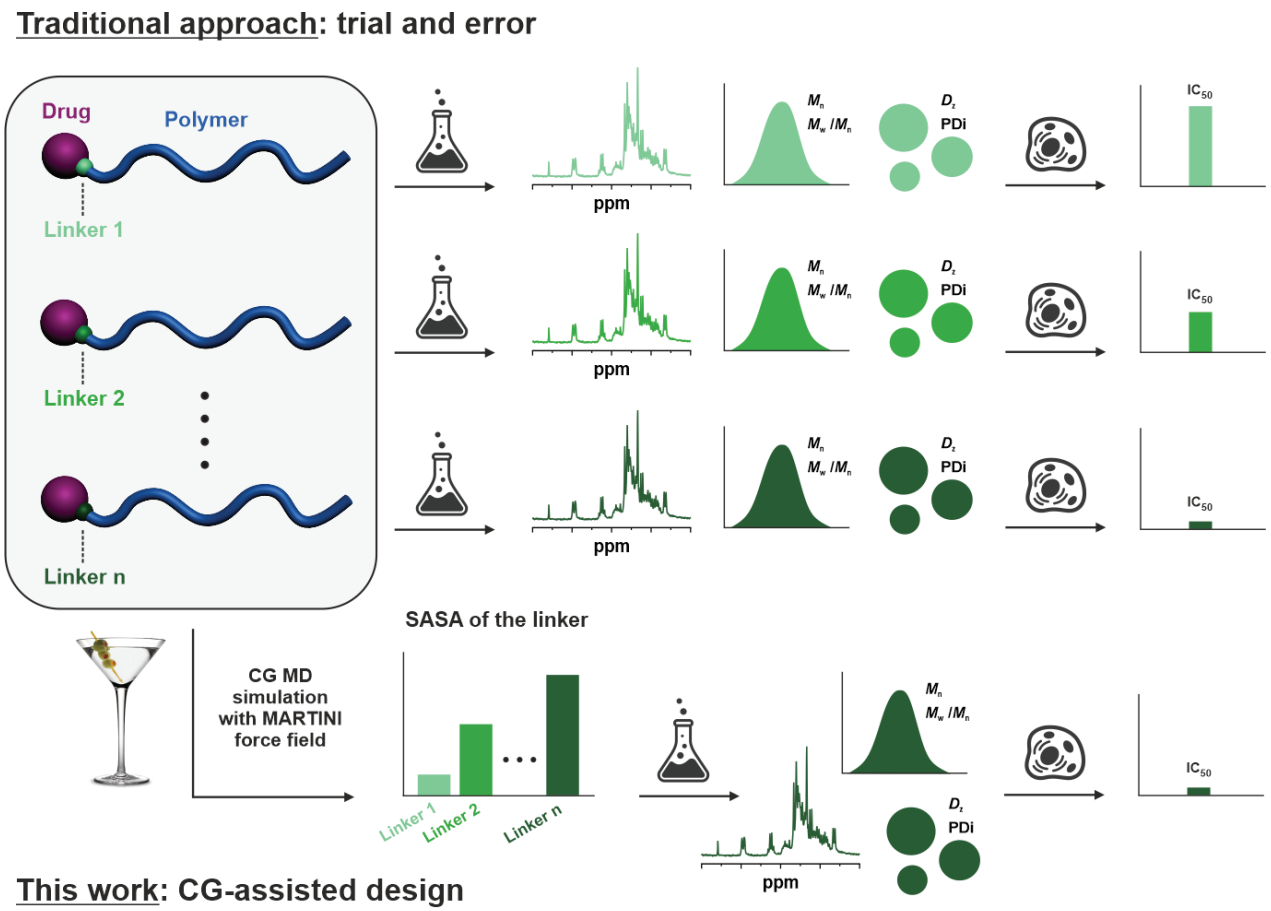

Figure 1. Schematic representation of the traditional trial-and-error approach and our coarse-grained (CG) molecular dynamic (MD) assisted design of polymer prodrug nanoparticles with optimized cytotoxicity. M_n = number-average molar mass; M_w/M_n = weight-average molar mass / number-average molar mass (dispersity); D_z = intensity average diameter; PDI = polydispersity index; IC_{50} = half maximal inhibitory concentration; SASA = solvent accessible surface area.

Methods

Theoretical part

The chemical structures of the different polymer prodrugs studied in this work are displayed in Figure 2. The coarse-grained models were built by following the procedure for parameterization of any coarse-grained

molecule as described in the tutorials available from the official MARTINI Web site (http://cgmartini.nl). Based on our previously reported coarse-grained models of Gem-based and Ptx-based PI prodrugs,[35] we applied this modeling to similar polymer prodrugs equipped with diglycolate-tetra(ethylene glycol) (*digly*-TEG) as a more hydrophilic linker (Gem-*digly*-TEG-PI and Ptx-*digly*-TEG-PI). Thanks to the transferable building block philosophy of MARTINI force fields, coarse-grained models of these new polymer prodrugs made from the same components (e.g., Gem, Ptx, *propa*/*amide*, *digly*, PI) can be easily derived without reparameterization. The coarse-grained modeling procedure of the *digly*-TEG linker was decomposed into four steps described below, and its parameters will be used for both Gem-*digly*-TEG-PI and Ptx-*digly*-TEG-PI polymer prodrugs.

All-atom model as reference

The initial three-dimensional structure of the *digly*-TEG linker (Figure S1a) was created with MarvinSketch 6.2.1 software from ChemAxon (http://www.chemaxon.com). It was then edited using UCSF Chimera 1.11.2 to add AM1-BCC atomic charges.[38] The python-based ACPYPE tool[39] was used to generate the topology and parameter file for the generalized AMBER force field (GAFF).[40] Then the *digly*-TEG linker was placed into a cubic simulation box of size equal to the solute largest dimension plus twice 1.4 nm to prevent the solute from interacting with its virtual images caused by the periodic boundary conditions. The box was further filled with octanol molecules. After minimizing its potential energy, the system was equilibrated with two 1 ns MD simulations, first in the NVT ensemble (constant Number of particles, Volume, and Temperature) by using the Berendsen coupling algorithm,[41] and then in the NPT ensemble (constant Number of particles, Pressure, and Temperature) by using the Nose-Hoover[42,43] and Parrinello-Rahman coupling methods.[44] Finally, the equilibrated system was submitted to a 20 ns production run under the same conditions as in the second equilibration step (T = 300 K and P = 1 bar), with the time constants τ_T = 0.5 ps and τ_P = 2.5 ps. In this work, all MD simulations were performed with the GROMACS 2019.1 software.[45] The electrostatic interactions were treated by using the smooth PME method[46] and the Lennard-Jones potentials were cut off at a distance of 1.2 nm. The length of all covalent bonds involving hydrogen atoms was kept constant using the LINCS procedure,[47] allowing a time step of 2 fs.

From all-atom to coarse-grained model

The mapping of the *digly*-TEG linker's all-atom model into its coarse-grained counterpart follows the three or four-to-one mapping procedure of MARTINI 2.0 force field. The bead types were chosen based on previous MARTINI models for small molecules[48] and are shown in Figure S1a.

Coarse-grained bonded parameters

The coarse-grained bonded parameters of the *digly*-TEG linker were determined from its all-atom simulation as follows: first, the distances between the centers of mass of two chemically connected beads and the valence angles between two pseudo covalent bonds were calculated and analyzed by using the *gmx distance*, *gmx angle* and *gmx analyze* GROMACS tools. In parallel, a first coarse-grained model was built with a set of initial bonded parameters alongside non-bonded parameters extracted from the publicly available *martini v2.1-dna peg.itp* and *martini v2.0 solvents.itp* files. An initial coarse-grained structure of *digly*-TEG linker was generated on the last frame of its all-atom simulation, and was further solvated in coarse-grained octanol.[48] After a minimization of 10000 steps, the coarse-grained system was first relaxed with a 250 ps simulation with a small time step of 5 fs, then equilibrated for 20 ns at T = 300 K and P = 1 bar by using the v-rescale temperature coupling[49] and Parrinello-Rahman pressure coupling methods[44] with the constants τ_T = 1.0 ps and τ_P = 12.0 ps. All non-bonded interactions were cut off above a distance of 1.1 nm and the electrostatic ones were treated by using the reaction-field (RF) method[50] with a relative dielectric constant ϵ_r = 15. The bond length and valence angle distributions of the coarse-grained trajectory were computed by using the same GROMACS tools as previously described in all-atom model and further compared with those calculated from the all-atom simulation. The coarse-grained bonded parameters were then iteratively adjusted until the bond length and valence angle distributions satisfactorily matched those of the all-atom model (Figure S1d). The obtained bonded parameters for *digly*-TEG linker are reported in Tables S1-S2. In this coarse-grained model, all dihedral angles have energy barriers set to zero.

Validation of the coarse-grained model with partition coefficient

The octanol-water partition coefficient P_{ow} is related to the octanol → water transfer free energy as: $\mathrm{Log}P_{ow} = \Delta G_{ow}/(2.303RT)$, with $\Delta G_{ow} = \Delta G_w - \Delta G_o$ where ΔG_w and ΔG_o are the solute solvation free energy in water and

octanol respectively. T is the temperature and R is the molar gas constant (8.314 $J.K^{-1}.mol^{-1}$). In this work, the transfer free energy ΔG_{ow} was calculated by using the umbrella sampling (US) technique,[51] in which a series of MD simulations were performed to pull the solute from the bulk of water to the bulk of octanol, by restraining the solute positions along a reaction coordinate via harmonic bias potentials. First, a 12 x 12 x 24 nm^3 rectangular box was considered, whose one half was filled with coarse-grained water and the other one with coarse-grained octanol (Figure S1b). The solute was initially put in the center of the water box. After a minimization of 100000 steps, the biphasic system was submitted to a 10 ns relaxation step with the v-rescale temperature coupling. Then a series of configurations were generated by pulling the solute from the water box (ξ = 6 nm) to octanol box (ξ = 12 nm) with an increment of 0.2 nm. The solute position was restrained in the center of each window with a force constant of 1000 kJ/mol/nm^2. A sequence of pulling, energy minimization, and 100 ps equilibration was performed to generate the system initial configurations. Then a 5 ns production run was performed for each window. After that, the octanol-water transfer free energy ΔG_{ow} was estimated from the solute potential of mean force (PMF) along the reaction coordinate extracted with the weighted histogram analysis method (WHAM)[52] (Figure S1c).

The octanol-water transfer free energy ΔG_{ow} and partition coefficient $\text{Log}P_{ow}$ of the *digly* and *digly*-TEG linkers calculated by this method are shown in Table 1, and compared with theoretical values provided by the XLOGP3 program.[53] The $\text{Log}P_{ow}$ value of the *digly*-TEG linker was slightly lower than that of the *digly* moiety, in good agreement with XLOGP3 values, confirming that *digly*-TEG is more hydrophilic than *digly* since the TEG moiety introduces more hydrogen bond acceptor groups.

Table 1. Octanol-water transfer free energy ΔG_{ow} and partition coefficient $\text{Log}P_{ow}$ of *digly* and *digly*-TEG linkers computed by umbrella sampling. † $\text{Log}P_{ow}$ predicted values by the XLOGP3 program.[53] ‡ Values from our previous work.[35]

Linker	ΔG_{ow} (kJ/mol)	$\text{Log}P_{ow}$	$\text{Log}P_{ow}$ (XLOGP3 †)
digly ‡	-8.4 ± 0.3	-1.5 ± 0.1	-0.1
digly-TEG	-8.9 ± 0.7	-1.6 ± 0.1	-0.5

Coarse-grained MD simulation of polymer prodrug self-assembly

The parameters of the validated *digly*-TEG coarse-grained model were then combined with those of the other polymer prodrug components (Gem, Ptx, PI and SG1)[35] to generate the coarse-grained model of new polymer prodrugs based on the *digly*-TEG moiety. For both polymer prodrugs (Gem-*digly*-TEG-PI_{20} and Ptx-*digly*-TEG-PI_{20}, where PI_{20} denotes a polyisoprene chain of 20 repeat units), an initial configuration was built by randomly placing 72 chains into a cubic box to reach a solute concentration of 5 mM. After a minimization of 50000 steps, MARTINI non-polarizable water beads W were added to fill the box. 15% of these W beads were replaced by anti-freeze water beads (WF),[48] and an appropriate number of them by sodium chloride ions to reach the physiological concentration of 150 mM. The system was first minimized with 50000 steps, then submitted to a 10 ns equilibration and a 15 μs production run under the same conditions as for the coarse-grained simulation of *digly*-TEG and previous polymer prodrugs.[35] All simulations were performed twice with different initial random atomic velocities.

Trajectories were analyzed by using GROMACS tools. The polymer prodrug aggregation process was monitored by calculating the number of aggregates and the number of chains in the largest aggregate as function of time by using *gmx clustsize* with a cut-off distance set to 0.5 nm. The aggregate diameter was calculated with *gmx gyrate*. The spatial localization of each component within the polymer prodrug nanoparticles was quantified by the radial distribution function *g(r)* of the center of mass (COM) of each component relative to the COM of the nanoparticle by using *gmx rdf*. The latter was also used to compute the distance between component pairs in aggregates. The solvent-accessible surface area (SASA) of the cleavage sites (amide and ester bonds) of the polymer prodrug under the form of nanoparticles was determined by using *gmx sasa* with a probe radius of 0.26 nm.[54]

Free energy profile of drug release from polymer prodrug nanoparticles

Umbrella Sampling simulations were employed to estimate the free energy profile during the release of one drug molecule from a polymer prodrug nanoparticle. A previously formed polymer prodrug nanoparticle in which all *digly*-TEG linker *sites 2* were cleaved was placed in a new 15 x 15 x 30 nm rectangular box and solvated with solvent (W and WF) and NaCl (150 mM). The system was first minimized (5000 steps) and

equilibrated with a 20 ns NPT simulation under the same conditions as in CG MD described above. A randomly selected Gem-*digly* or Ptx-*digly* moiety (cleaved at *site 2*) was then pulled from the nanoparticle along the *distance* coordinates ξ by using a default harmonic force constant of 1000 $kJ \cdot mol^{-1} \cdot nm^{-2}$ to generate a series of initial configurations. The minimum distance between the COM of the drug-*digly* and the COM of the nanoparticle is the radius of gyration of the nanoparticle. In each window, the energy of the system was minimized (5000 steps), equilibrated during 20 ns in NVT ensemble, and simulated during 50 ns in the NPT ensemble, using the same conditions as in CG MD described above. The weighted histogram analysis method (WHAM) was used to compute the PMF profile of the drug-*digly* unbinding (i.e., release) process which was corrected by adding the term $k_B T \ln(4\pi\xi^2)$ to compensate for the decrease in entropic free energy term due to the increase in the number of system configurations as the distance ξ increases.[55]

Experimental part

Materials

2-bromo propionic acid (> 98 %), diglycolic anhydride (> 98 %) and tetraethylene glycol (TEG, > 95 %) were purchased from TCI EUROPE (France), Copper powder (< 425 μm), pentamethyldiethylenetriamine (PMDETA) (99 %), 4-(dimethylamino)pyridine (≥ 99 %), triethylamine (≥ 99.5 %), *N,N*-diisopropyl ethylamine (≥ 99 %), *N*-(3-dimethylaminopropyl)-*N'*-ethylcarbodiimide hydrochloride) (EDC·HCl) (commercial grade), isoprene (99 %), Tween 80, benzotriazol-1-yloxytripyrrolidinophosphonium hexafluorophosphate) (PyBOP) (≥ 97 %), human serum, theophylline (≥ 99 %), phosphate-buffered saline, tetrazolium salt (3-(4,5-dimethylthiazol-2-yl)-2,5-diphenyltetrazolium bromide) (MTT) (98 %), Dulbecco's phosphate buffered saline, Dulbecco's modified eagle's medium (DMEM) and RPMI-1640 medium, trypsin-EDTA solution, all the salt compounds and anhydrous solvents were purchased from Sigma-Aldrich (France) and used as received. Tetrahydrouridine (≥ 90 %) was purchased from EMD Millipore Corporation. Ethylene glycol (≥ 99.5 %) was purchased from Fluka Analytical. Gemcitabine·HCl (> 98 %) was purchased from Carbosynth Limited (UK). Paclitaxel (> 95 %) was purchased from Sequoia Research Products Limited. Fetal bovine serum (FBS) was purchased from Dulbecco (Gibco, France). Penicillin was purchased from Lonza (Verviers, Belgium). Deuterated chloroform ($CDCl_3$) (99.80 % D, water < 0.01 %) was obtained from Eurisotop. Hydrochloric acid

37 % and all the solvents at the highest grade were purchased from Carlo Erba Reagents. *N-tert*-butyl-*N*-[1-diethylphosphono-(2,2-dimethylpropyl) nitroxide] (SG1, 85 %) was mainly kindly supplied by Arkema. Glycol-AMA-SG1, *digly*-AMA-SG1, Ptx-*digly*-AMA-SG1 and Gem-AMA-SG1 were synthesized as published elsewhere.[36,56]

Analytical Methods

Nuclear magnetic resonance spectroscopy (NMR). NMR spectroscopy was performed in 5 mm diameter tubes in $CDCl_3$ at 25 °C. ^{1}H and ^{13}C NMR spectroscopy was performed on a Bruker Avance 300 spectrometer at 300 MHz and 75 MHz, respectively. ^{19}F and ^{31}P NMR spectroscopy were performed on a Bruker Avance 200 spectrometer at 188 MHz and 161.1 MHz respectively. The chemical shift scale of $CDCl_3$ was calibrated on the basis of the internal solvent signals (δ = 7.26 ppm).

Mass spectrometry. Mass spectra were performed on a Bruker Esquire-LC instrument with a 1260 infinity ultrahigh pressure liquid chromatography (UHPLC) system with UV visible (with PDA diode array) and a quadrupole time-of-flight (Q-TOF) mass spectrometer (Agilent Technologies).

Size exclusion chromatography (SEC). SEC was performed on a system equipped with two columns from Agilent (PL-gel MIXED-D; 300 x 7.5 mm; bead diameter of 5 μm; linear part 400 to 4 x 10^5 g·mol^{-1}) thermostated at 30 °C, a differential refractive index detector (Spectra System RI150, Thermo Electron Corp), a Waters 515 HPLC pump at a flow rate of 1 mL.min^{-1} and chloroform as the eluent. Toluene was used as a flow-rate marker. The calibration curve was based on polystyrene (PS) standards (peak molar masses, M_p = 575–126500 g.mol^{-1}) from Agilent. A PI calibration curve was obtained by converting the PS standard peak molecular weights (MPS) to PI molecular weights (MPI) using Mark-Houwink-Sakurada (MHS) constants determined for both polymers in CCl_4 at 25 °C. For PI, the MHS constants used were K_{PI} = 2.44 × 10^{-4} and α_{PI} = 0.712. For PS, K_{PS} = 7.1 × 10^{-4} and α_{PS} = 0.54 (M_w < 16700 g.mol^{-1}) or K_{PS} = 1.44 × 10^{-4} and α_{PS} = 0.713 (M_w > 16700 g.mol^{-1}).[57] This technique allowed M_n (number-average molar mass), M_w (weight-average molar mass), and M_w/M_n (dispersity, $Đ$) to be determined.

Dynamic light scattering (DLS) and zeta potential measurement. Nanoparticles' average diameter (D_z) and zeta potential (ζ) were recorded by DLS with a Zetasizer Ultra from Malvern (multi-angle, 173°, 13°, 90°) at a temperature of 25 °C.

Cryogenic-transmission electron microscopy (cryo-TEM). The morphology of the nanoparticles was observed by cryo-TEM. Briefly, 5 μL of the nanoparticle suspension (2.5 mg·mL^{-1} of Gem-*digly*-TEG-PI or 4 mg·mL^{-1} of Ptx-*digly*-TEG-PI) was deposited on a Lacey Formvar/carbon 300 mesh copper microscopy grid (Ted Pella). Most of the drop was removed with a blotting filter paper and the residual thin film remaining within the holes was vitrified by plunging into liquid ethane. Samples were then observed using a JEOL Model 2100HC microscope.

High-performance liquid chromatography (HPLC). The drug (Gem or Ptx) release kinetics was quantified by HPLC (Waters, Milford, MA, USA). The chromatographic system was composed of a Waters 1525 Binary HPLC pump, a Waters 2707 Autosampler, a C18 Uptisphere column (3 µm, 150 x 4.6 mm; Interchim), an HPLC column temperature controller (model 7950 column heater and chiller; Jones Chromatography, Lakewood, CO) and a Waters 2998 programmable photodiode-array detector. The HPLC column was maintained at 30 °C. Detection of Gem and Ptx was monitored at 270 nm and 227 nm, respectively.

Synthesis methods

Synthesis of AMA-SG1. AMA-SG1 was synthesized as published elsewhere[58] with optimized purification conditions. SG1 (0.94 g, 2.7 mmol, 1.08 eq) and 2-bromo propionic acid (0.38 g, 2.5 mmol, 1 eq) were dissolved in 5 mL acetonitrile to keep the concentration of alkyl bromide as 0.5 mM. Copper powder (160 mg, 2.5 mmol, 1 eq) was added into solution and then degassed with argon for 15 min. Then PMDETA (0.5 g, 3.0 mmol, 1.2 eq) was added dropwise into the solution leading to a color change from orange to dark green. The reaction was stirred at room temperature for 16 h resulting in the formation of green precipitate. The mixture was poured into 50 mL NaOH (1 M, pH = 12), then washed three times with 30 mL diether ethyl. The aqueous phase was acidified with 1 M HCl until pH = 1 to get a light green solution, then extracted three times with 30 mL dichloromethane. The final product was dried over $MgSO_4$ and the solvent was removed by rotary evaporation to give AMA-SG1 as colorless solid (0.74 g, yield = 80 %). ^{1}H NMR (300 MHz, $CDCl_3$): mixture of diastereomers: δ 4.70 and 4.55 (*q*, *J* = 6.7 Hz and 6.9 Hz, 1H), 4.34–4.17 and 4.17–4.00 (*m*, 4H), 3.43 and 3.34 (*d*, *J* = 1.4 Hz and 1.3 Hz, 1H), 1.61 and 1.49 (*dd*, *J* = 6.9, 1.3 Hz and *J* = 7.0, 1.3 Hz, 3H), 1.39–1.27 (*m*, 6H), 1.20 and 1.19 (2*s*, 9H), 1.18 and 1.13 (2*s*, 9H) ppm. ^{13}C NMR (75 MHz, $CDCl_3$): mixture of diastereomers: δ 174.94, 174.21, 81.59, 80.96, 69.81 (*d*, *J* = 98.4 Hz), 67.96 (*d*, *J* = 95.5 Hz), 62.99, 62.73

(*d*, *J* = 7.1 Hz), 62.54, 62.41 (*d*, *J* = 6.7 Hz), 60.78 (*d*, *J* = 8.1 Hz), 60.27 (*d*, *J* = 7.6 Hz), 35.77, 35.72, 30.42 (*d*, *J* = 6.0 Hz, 3C), 30.15 (*d*, *J* = 6.0 Hz, 3C), 27.85 (3C), 27.71 (3C), 18.68, 18.29, 16.46 (*d*, *J* = 5.9 Hz), 16.28 (*d*, *J* = 6.1 Hz), 16.19, 16.15 ppm. ESI-MS (M + H^+): 368.2202. Calculated for $C_{16}H_{35}NO_6P^+$: 368.21.

Synthesis of *digly*-TEG-AMA-SG1. AMA-SG1 (0.3672 g, 1.0 mmol, 1 eq), DMAP (0.244 g, 2.0 mmol, 2 eq), and EDC·HCl (0.3887 g, 2.0 mmol, 2 eq) were dissolved in anhydrous dichloromethane (DCM, 33 mL) and then poured in a round bottom flask further degassed under argon atmosphere at room temperature for 20 min. Then TEG (0.778 g, 4.0 mmol, 4 eq) was dissolved in anhydrous DMF (6.7 mL) and added dropwise into the flask. After stirring at 30 °C for 24 h, the crude product was poured into 150 mL of EtOAc, then washed with saturated $NaHCO_3$ aqueous solution, 10 % HCl and brine. The product was dried over $MgSO_4$ and concentrated under reduced pressure, followed by purification by flash chromatography on silica gel (DCM/methanol; from 98/2 to 94/6, v/v) to yield a colorless oily product TEG-AMA-SG1 (0.46 g, yield = 84 %). ^{1}H NMR (300 MHz, $CDCl_3$): mixture of diastereomers: *δ* 4.60 (*dq*, *J* = 14.1, 6.9 Hz, 1H), 4.27–3.85 (*m*, 6H), 3.73–3.54 (*m*, 14H), 3.33 and 3.24 (*d*, *J* = 26.7 Hz and 25.5 Hz, 1H), 1.49 and 1.46 (*d*, *J* = 7.0 Hz and 7.0 Hz, 3H), 1.30–1.20 (*m*, 6H), 1.14 and 1.12 (2*s*, 9H), 1.10 and 1.07 (2*s*, 9H) ppm. ^{13}C NMR (75 MHz, $CDCl_3$): major diastereomer: *δ* 173.90, 82.72, 72.62, 70.72, 70.60 (2C), 70.54, 70.40, 69.03, 63.45, 62.24 (*d*, *J* = 6.8 Hz), 61.70, 61.5, 59.28 (*d*, *J* = 7.4 Hz), 35.34 (*d*, *J* = 5.1 Hz), 30.27 (*d*, *J* = 6.0 Hz, 3C), 28.07 (3C), 18.00, 16.55 (*d*, *J* = 6.0 Hz), 16.23 (*d*, *J* = 6.9 Hz) ppm. ESI-MS (M + Na^+): 566.3080. Calculated for $C_{24}H_{50}NO_{10}PNa^+$: 567.31.

The obtained TEG-AMA-SG1 (0.326 g, 0.6 mmol, 1 eq) was mixed with diglycolic anhydride (0.174 g, 1.5 mmol, 1.25 eq) and triethylamine (0.42 mL, 0.3036 g, 3.0 mmol, 5 eq) in anhydrous DCM (3 mL). The reaction mixture was stirred at room temperature for 4 h under an argon atmosphere. The reaction mixture was then poured into DCM (25 mL) and the organic phase was washed with 1 M HCl and brine before being dried over $MgSO_4$. The residue was concentrated under reduced pressure to yield a colorless sticky solid *digly*-TEG-AMA-SG1 (0.34 g, yield = 86 %). ^{1}H NMR (300 MHz, $CDCl_3$): mixture of diastereomers: *δ* 4.56 (*q*, *J* = 7.2 Hz, 1H), 4.33–3.86 (*m*, 12H), 3.75–3.63 (*m*, 4H), 3.62–3.57 (*m*, 8H), 3.30 (*dd*, *J* = 28.8, 26.1 Hz, 1H), 1.45 (*dd*, *J* = 6.9, 5.2 Hz, 3H), 1.31–1.18 (*m*, 6H), 1.13 and 1.11 (2*s*, 9H), 1.08 and 1.07 (2*s*, 9H). ^{13}C NMR (75 MHz, $CDCl_3$): major diastereomer: *δ* 172.42, 170.95, 170.15, 82.74, 70.72, 70.58 (3C), 70.51, 70.42, 68.95, 68.84, 68.23, 63.90, 62.44 (*d*, *J* = 6.5 Hz), 61.75, 61.56, 59.73 (*d*, *J* = 7.7 Hz), 35.35 (*d*, *J* = 4.8 Hz),

30.13 (*d*, *J* = 6.1 Hz, 3C), 27.98 (3C), 17.95, 16.43 (*d*, *J* = 4.4 Hz), 16.13 (*d*, *J* = 6.9 Hz) ppm. ESI-MS (M + H^+): 660.3438. Calculated for $C_{28}H_{55}NO_{14}P^+$: 660.33.

Synthesis of Gem-*digly*-AMA-SG1. Gem·HCl (0.20 g, 0.68 mmol, 1 eq) and DIPEA (*N,N*-diisopropylethylamine) (115 *μ*L, 0.68 mmol, 1 eq) were dissolved in anhydrous DMF (5 mL), and degassed by argon for 10 min, then *digly*-AMA-SG1 (0.68 mmol, 0.36 g, 1 eq), PyBOP (0.356 g, 0.68 mmol, 1 eq) were dissolved in dry DMF (5 mL), then added dropwise into the solution of Gem by syringe. DIPEA (345 *μ*L, 2.0 mmol, 3 eq) was then added into the reaction mixture dropwise, followed by stirring under argon atmosphere at room temperature for 24 h. The mixture was then poured into 50 mL of EtOAc and the organic phase was washed with 10 % HCl, saturated $NaHCO_3$ and brine, before being dried over $MgSO_4$. The residue was then concentrated under reduced pressure and purified by flash chromatography on silica gel (DCM/methanol; from 94/6 to 92/8, v/v) to get colorless sticky solid (0.23 g, yield = 43 %). ^{1}H NMR (300 MHz, $CDCl_3$): mixture of diastereomers: *δ* 8.28 (*d*, *J* = 8.3 Hz, 1H), 7.43 (*d*, *J* = 7.3 Hz, 1H), 6.30 (*t*, *J* = 7.0 Hz, 1H), 4.68–4.16 (*m*, 12H), 4.15–3.87 (*m*, 6H), 3.33 (*dd*, *J* = 25.9, 21.3 Hz, 1H), 1.47 (*dd*, *J* = 7.1, 7.0 Hz, 4H), 1.35–1.24 (*m*, 8H), 1.18 and 1.16 (2*s*, 9H) 1.14 and 1.12 (2*s*, 9H) ppm (see Figure S2a). ^{13}C NMR (75 MHz, $CDCl_3$): mixture of diastereomers: 172.75, 169.80, 169.57, 162.18, 155.51, 145.49, 122.64, 97.12, 85.35, 82.50, 81.61, 71.25, 70.23, 68.59 (*d*, *J* = 12.6 Hz), 63.11, 62.61 (*d*, *J* = 24.0 Hz), 61.93 (2C), 59.64, 59.38 (*d*, *J* = 7.7 Hz), 35.49 (*d*, *J* = 4.6 Hz), 30.15 (*d*, *J* = 9.5 Hz, 3C), 28.21 (3C), 19.47, 16.65 (*d*, *J* = 5.9 Hz), 16.30 (*d*, *J* = 2.7 Hz) ppm. ^{19}F NMR (188 MHz, $CDCl_3$): -118.65 ppm. ESI-MS (M + H^+): 773.3194. Calculated for $C_{31}H_{52}F_2N_4O_{14}P^+$: 773.31.

Synthesis of Gem-*digly*-TEG-AMA-SG1. Gem·HCl (0.090 g, 0.30 mmol, 1 eq) and DIPEA (80 *μ*L, 0.30 mmol, 1 eq) were dissolved in anhydrous DMF (2.4 mL). *digly*-TEG-AMA-SG1 (0.200 g, 0.30 mmol, 1 eq) and PyBOP (0.156 g, 0.30 mmol, 1 eq) were dissolved in anhydrous DMF (2.4 mL), then dropwise added to the Gem solution by syringe. DIPEA (94 *μ*L, 0.78 mmol, 2.6 eq) was added dropwise into mixture, followed by stirring under argon atmosphere at room temperature for 24 h. The reaction mixture was then poured into EtOAc (50 mL) and the organic phase was washed with 10 % HCl, saturated $NaHCO_3$ and brine before being dried over $MgSO_4$. Finally, the residue was concentrated under reduced pressure and purified by flash chromatography (SiO_2, DCM/MeOH = 20/1 to 90/10) to get colorless sticky solid (0.098 g, yield = 36 %) ^{1}H NMR (300 MHz, $CDCl_3$): mixture of diastereomers: *δ* 8.33 (*dd*, *J* = 17.1, 7.7 Hz, 1H), 7.40 (*d*, *J* = 7.5 Hz, 1H), 6.25 (*d*, *J* = 7.3 Hz, 1H), 4.65–4.46 (*m*, 1H), 4.49–3.80 (*m*, 16H), 3.72–3.52 (*m*, 12H), 3.35 and 3.26 (*dd*, *J* =

25.3 Hz, 24.9 Hz, 1H), 1.46 (*dd*, *J* = 7.1, 3.4 Hz, 3H), 1.26 (*dt*, *J* = 11.1, 7.0 Hz, 6H), 1.15 and 1.13 (2*s*, 9H), 1.12 and 1.06 (2*s*, 9H) ppm (see Figure S2b). ^{13}C NMR (75 MHz, $CDCl_3$): mixture of diastereomers: *δ* 173.68, 169.42, 169.18, 161.50, 155.79, 145.40, 122.17, 96.90, 85.05, 82.67, 71.12, 70.68 (4C), 69.08, 68.91 (2C), 68.67, 68.45 (*d*, *J* = 10.4 Hz), 64.51, 63.57, 62.40, 61.92, 61.72, 59.60, 59.36 (*d*, *J* = 16.8 Hz), 35.62 (*d*, *J* = 28.8 Hz), 29.67 (*d*, *J* = 6.0 Hz, 3C), 28.10 (3C), 19.53, 16.44 (*d*, *J* = 6.0 Hz), 16.11 (*d*, *J* = 6.4 Hz) ppm. ^{19}F NMR (188 MHz, $CDCl_3$) *δ* -118.64 ppm. ESI-MS (M + H^+): 905.3966, Calculated for $C_{37}H_{64}F_2N_4O_{17}P^+$: 905.39.

Synthesis of Ptx-*digly*-TEG-AMA-SG1. *Digly*-TEG-AMA-SG1 (0.100 g, 0.15 mmol, 1.3 eq), DMAP (0.028 g, 0.23 mmol, 2 eq) and EDC·HCl (0.044 g, 0.23 mmol, 2 eq) were dissolved in anhydrous DCM (5 mL), poured into a round bottom flask and degassed under argon atmosphere at room temperature for 15 min. A solution of Ptx (0.098 g, 0.115 mmol, 1 eq) in anhydrous DCM (1 mL) was added dropwise into the flask and the mixture was stirred at 30 °C for 22 h. The crude was then poured into EtOAc (30 mL) and the organic phase was washed with brine before being dried over $MgSO_4$. The residue was concentrated under reduced pressure and purified by flash chromatography on silica gel (from EtOAc to EtOAc/MeOH; 98/2, v/v) to yield a white solid (0.156 g, yield = 70 %) ^{1}H NMR (300 MHz, $CDCl_3$): mixture of diastereomers: *δ* 8.14 (*d*, *J* = 7.1 Hz, 2H), 7.75 (*d*, *J* = 7.1 Hz, 2H), 7.66–7.29 (*m*, 11H), 7.07 (*d*, *J* = 9.1 Hz, 1H), 6.35–6.20 (*m*, 2H), 6.03 (*d*, *J* = 9.7 Hz, 1H), 5.68 (*d*, *J* = 6.6 Hz, 1H), 5.59 (*t*, *J* = 2.9 Hz, 1H), 4.97 (*d*, *J* = 9.3 Hz, 1H), 4.59 (*q*, *J* = 6.7 Hz, 1H), 4.50–3.89 (*m*, 14H), 3.82 (*d*, *J* = 6.7 Hz, 1H), 3.73–3.54 (*m*, 12H), 3.26 (*d*, *J* = 25.7 Hz, 1H), 2.63–2.32 (*m*, 6H), 2.22 (*s*, 3H), 2.19–2.12 (*m*, 1H), 1.94 (*s*, 3H), 1.90–1.77 (*m*, 2H), 1.68 (*s*, 3H), 1.50 (*d*, *J* = 6.7 Hz, 3H), 1.34–1.19 (*m*, 9H), 1.13 (*m*, 24H) ppm (see Figure S3b). ^{13}C NMR (75 MHz, $CDCl_3$): mixture of diastereomers: *δ* 203.75, 173.91, 171.12, 169.84, 169.51, 169.00, 167.63, 167.17, 167.02, 142.57, 136.79, 133.60, 132.95, 131.95, 130.23 (2C), 129.28, 129.12 (2C), 128.71 (2C), 128.65 (2C), 128.54, 127.23 (2C), 126.58 (2C), 84.45, 82.57, 81.11, 79.15, 76.45, 75.57, 75.17, 74.44, 72.08 (2C), 70.53 (4C), 68.96, 68.82, 68.19, 67.98, 64.03, 63.36, 61.57, 60.34, 58.53, 52.75, 45.60, 43.20, 35.57 (*d*, *J* = 11.1 Hz), 35.32 (*d*, *J* = 4.9 Hz), 30.21 (*d*, *J* = 6.0 Hz), 29.63 (*d*, *J* = 3.7 Hz), 28.01 (2C), 27.95, 26.82, 22.69, 22.65, 22.13, 20.76, 19.36, 17.91, 16.47 (*d*, *J* = 6.0 Hz), 16.16 (*d*, *J* = 6.8 Hz), 14.75, 9.59 ppm. ESI-MS (M + H^+): 1495.6572. Calculated for $C_{75}H_{104}N_2O_{27}P^+$: 1495.65.

Synthesis of Gem-based polymer prodrugs. The synthesis of Gem-*amide*-PI, Gem-*digly*-PI and Gem-*digly*-TEG-PI were synthesized as follows. A solution of the corresponding Gem-based alkoxyamine (Gem-*amide*-AMA-SG1, Gem-*digly*-AMA-SG1 and Gem-*digly*-TEG-AMA-SG1, respectively) was prepared by mixing the Gem-based alkoxyamine (0.04 mmol), isoprene (0.8 mL, 8.0 mmol) and dioxane (0.8 mL). The mixture was transferred to a 15 mL-capacity pressure tube (AceGlass 8648-164) and degassed by three consecutive freeze-pump-thaw cycles, then backfilled with argon. The tube was placed in an oil bath at 115 °C for 16 h, then cooled down to room temperature by placing it in an ice water bath. The conversion was calculated by gravimetry. Unreacted isoprene and dioxane were removed under reduced pressure and the obtained product was characterized by SEC and NMR.

Synthesis of Ptx-based polymer prodrugs. The synthesis of Ptx-*digly*-PI and Ptx-*digly*-TEG-PI were synthesized as follows. A solution of the corresponding Ptx-based alkoxyamine (Ptx-*digly*-AMA-SG1 and Ptx-*digly*-TEG-AMA-SG1, respectively) was prepared by mixing the Ptx-based alkoxyamine (0.02 mmol), isoprene (0.4 mL, 4.0 mmol) and dioxane (0.4 mL). The mixture was transferred to a 15 mL-capacity pressure tube (Ace Glass 8648-164 and degassed by three consecutive freeze-pump-thaw cycles, then backfilled with argon. The tube was placed in an oil bath at 115 °C for 16 h, then cooled down to room temperature by placing it in an ice water bath. The conversion was calculated by gravimetry. Unreacted isoprene and dioxane were removed under reduced pressure and the obtained product was characterized by SEC and NMR.

Synthesis of PI. PI was also synthesized by following the above procedure. A solution of AMA-SG1 (0.08 mmol), isoprene (0.8 mL, 8.0 mmol) and dioxane (0.8 mL) was prepared. The mixture was transferred to a 15 mL-capacity pressure tube (Ace Glass 8648-164 and degassed by three consecutive freeze-pump-thaw cycles, then backfilled with argon. The tube was placed in an oil bath at 115 °C for 16 h, then cooled down to room temperature by placing it in an ice water bath. The conversion was calculated by gravimetry. Unreacted isoprene and dioxane were removed under reduced pressure and the obtained product was characterized by SEC and NMR.

Purification of the polymer prodrugs and PI. Purification was performed by dissolving the crude in 1 mL of DCM followed by precipitation in 30 mL of cold methanol and centrifugation at 10,000 rpm for 15 min. The solvents were removed under rotary evaporation and the product was further dried overnight under high vacuum.

Nanoparticle preparation

All polymer prodrug and PI nanoparticles were obtained at 1.0 mg.mL^{-1} by the nanoprecipitation technique. First, 1.0 mg of the polymer prodrug (Gem-*amide*-PI, Gem-*digly*-PI, Gem-*digly*-TEG-PI, Ptx-*digly*-PI, Ptx-*digly*-TEG-PI) or PI were placed into a 7 mL-glass vial to which were added 0.5 mL of THF. The solution was then added dropwise into 1.0 mL of deionized water under stirring at 350 rpm at room temperature. The THF was then removed by rotary evaporation at 35 °C for 30 min under stirring at 120 rpm to yield a stable nanoparticle suspension. The absence of residual THF was verified by ^{1}H NMR.

Drug release experiments

To increase the signal-over-noise ratio for low drug release fractions, the concentration of polymer prodrug nanoparticles was increased up to 2.5 mg.mL^{-1} for Gem-based polymer prodrug nanoparticles and to 4.0 mg.mL^{-1} for Ptx-based polymer prodrug nanoparticles by increasing the amount of polymer prodrugs during the nanoprecipitation, in agreement with the literature.[37,59]

For Gem-based polymer prodrug nanoparticles, 420 μL of each nanoparticle suspension were added to 1680 μL of PBS or human serum (containing 200 μg.mL^{-1} tetrahydrouridine). Aliquots (100 μL) of each reaction medium were incubated at 37 °C for different times (0, 1, 2, 4, 8, 24 and 48 h). Each sample was then spiked with 10 μL of theophylline (10 μM, internal standard) before addition of 1 mL of acetonitrile/methanol (90/10, v/v) mixture. The resulting mixture was then centrifuged (15,000 g, 20 min, 4 °C). The supernatant was evaporated to dryness under nitrogen flow for 1 h at 37 °C. The released Gem was quantified by HPLC. The mobile phase was composed of eluent A (methanol/0.05 M sodium acetate, 5/95, v/v) and eluent B (methanol/0.05 M sodium acetate, 97/3, v/v). The residues were dissolved in 100 μL eluent A and isocratic elution was performed for 8 min at a flow rate of 0.8 mL.min^{-1}, then 1 min linear gradient to reach 75 % eluent A, followed by 6 min isocratic elution. Then 1 min linear gradient to reach 100 % eluent B followed by 10 min isocratic elution and 1 min linear gradient to reach 100 % eluent A, then a 7 min-hold for equilibration back to initial conditions.

For Ptx-based polymer prodrug nanoparticles, 210 μL of each nanoparticle suspension were added to 1890 μL of PBS (containing 1 wt % Tween 80) or human serum. Aliquots (100 μL) of each reaction medium were incubated at 37 °C for different times (0, 1, 2, 4, 8, 24 and 48 h). To each sample were added 1 mL

acetonitrile/methanol (90/10, v/v) mixture. The resulting mixture was then centrifuged (15,000 g, 20 min, 4 °C). The supernatant was evaporated to dryness under vacuum at 30 °C. The released Ptx was quantified by HPLC. The mobile phase was composed of acetonitrile/water (70/30, v/v) mixture. The residues were dissolved in the mobile phase and subjected to isocratic elution for 7 min at a flow rate of 1.0 mL.min^{-1}. Then 1 min linear gradient to reach 95 % acetonitrile and 15 min of isocratic elution. Then was followed by 1 min linear gradient to acetonitrile/water (70/30, v/v), then a 6 min-hold for equilibration back to initial conditions.

Cell lines and cell culture

Murine leukemia cell line L1210 was kindly provided by Dr. Lars Petter Jordheim (Université Claude Bernard Lyon I, Lyon, France), and maintained as recommended. Human lung carcinoma cell line A549 was obtained from the American Type Culture Collection and maintained as recommended. Briefly, both cell lines were cultured in Dulbecco's minimal essential medium (DMEM). All media were supplemented with 10 % heat-inactivated FBS (56 °C, 30 min) and penicillin (100 U·mL^{-1}). Cells were maintained in a humid atmosphere at 37 °C with 5 % CO_2.

In vitro anticancer activity

The cytotoxicity of the polymer prodrug nanoparticles and the free drugs was evaluated by MTT [3-(4,5-dimethylthiazol-2-yl)-2,5-diphenyl tetrazolium bromide] viability test on A549 and L1210 cell lines. First, 100 μL cell suspension (with density of 4000 cells/well) were seeded into 96-well plate for 24 h incubation for A549 cells and for 1 h incubation for L1210 cells, then the cells were exposed to a series of concentrations of different polymer prodrug nanoparticles, control polymer nanoparticles (PI-SG1) or free drugs (Gem or Ptx) for 72 h. After drug exposition, the medium was added with 20 μL of MTT solution (5 mg·mL^{-1} in PBS) for each well. The plates were incubated for 1 h at 37 °C and the medium was removed (by centrifugation under 300 x *g* for 10 min for L1210 cells). Then 200 μL of DMSO were then added to each well to dissolve the purple formazan crystals. Absorbance was measured at 570 nm using a microplate reader (LAB Systems Original Multiscan MS, Finland). The percentage of cell viability was calculated as the absorbance ratio of treated to untreated cells. The half maximal inhibitory concentration (IC_{50}) was determined from the

percentage-dose curves by using a one-way ANOVA test with GraphPad Prism (version 8.0.2). All the MTT tests were set up in triplicate to determine the mean value and standard deviation.

Results and Discussions

General characteristics of polymer prodrug nanoparticles

The polymer prodrugs selected for improvement by coarse-grained model-assisted design were synthesized by the "*drug-initiated*" method (also termed "*grafting from*"),[60] which relies on the controlled growth of a polymer chain from a drug molecule. This synthetic strategy has emerged as a robust yet simple approach as it requires only a few synthesis steps with high yields, and it permits easy adjustment of the polymer chain length and thus the drug loading. It is also very versatile as the nature of the drug, the linker and the polymer can be independently changed to gives access to a broad range of polymer prodrugs with tunable physicochemical and biological properties.

Among the different structures deriving from this synthetic strategy reported to date, Gem-PI and Ptx-PI polymer prodrugs were among the most promising ones owing to their surfactant-free formulation into nanoparticles exhibiting significant cytotoxicity against various cancer cell lines and anticancer efficacy in tumor-bearing mice.[35-37] Two types of linkers were experimentally investigated at that time: an amide bond with Gem (Gem-*amide*-PI) and an ester-diglycolate sequence (*digly*) with Ptx (Ptx-*digly*-PI). Herein, to test our coarse-grained model-assisted design of polymer prodrugs in its ability to experimentally predict the influence of the nature of the linker on drug release and cytotoxicity, we simulated the supramolecular organization upon self-assembly of Gem- and Ptx-based prodrugs equipped with a novel, previously untested diglycolate-tetraethylene glycol (*digly*-TEG) linker. This linker was designed to increase drug release and thus cytotoxicity through its greater hydrophilicity and surface exposure using the TEG moiety (Figure 2). Additional simulations and experimental investigations were also performed to establish linker structure-supramolecular organization-drug release-cytotoxicity relationships based on a total of three different linkers per drug type: (i) Gem-*digly*-PI, to investigate potential increase in cytotoxicity compared to Gem-*amide*-PI due to the greater lability of *digly* and (ii) Ptx-*propa*-PI, which is suspected to prevent efficient drug release because of its high hydrophobicity and steric hindrance.

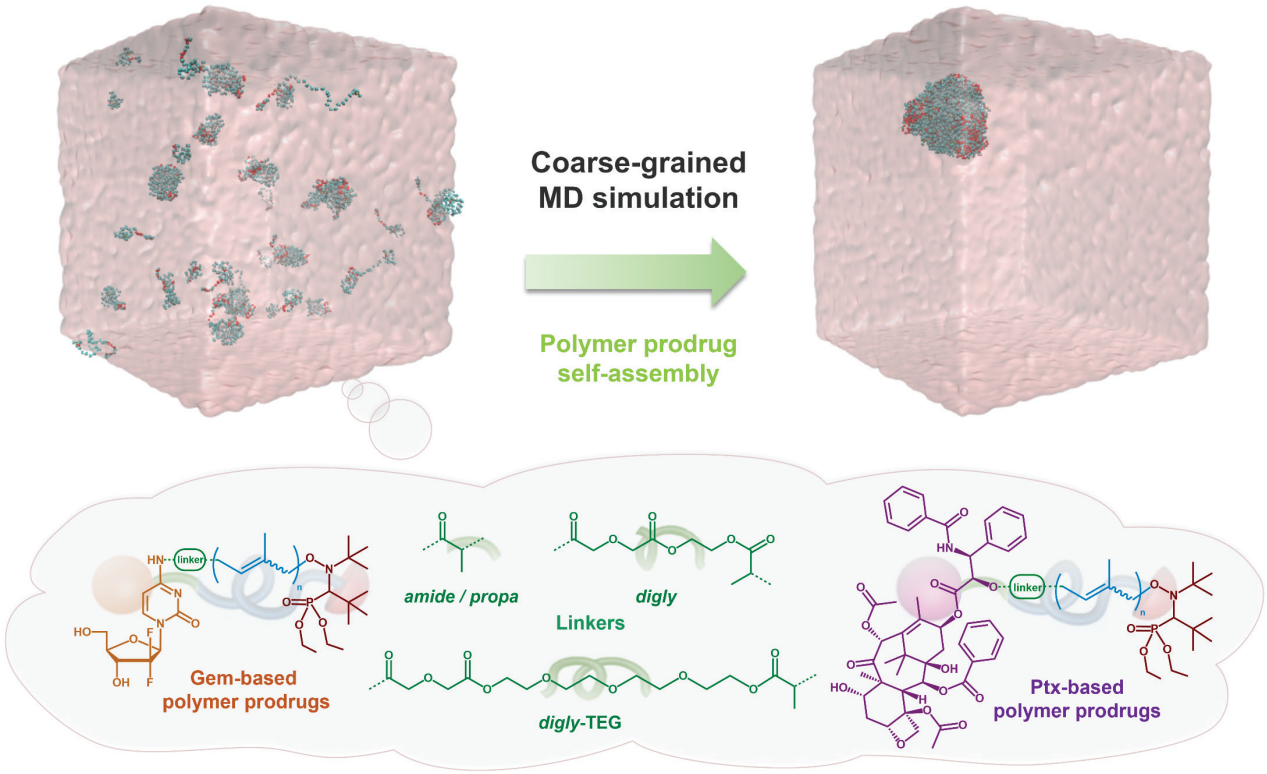

Figure 2. Coarse-grained molecular dynamic (MD) simulations of polymer prodrug self-assembly and chemical structures of the different polymer prodrugs and linkers investigated in this study. Gem = gemcitabine; Ptx = paclitaxel; TEG = tetra(ethylene glycol).

Coarse-grained simulations of polymer prodrug nanoparticles

The self-assembly process of Gem-*digly*-TEG-PI and Ptx-*digly*-TEG-PI polymer prodrugs was monitored by calculating the number of aggregates and the number of chains in the largest one in their duplicate trajectories (Figure S4a). Results show that the randomly dispersed chains self-assemble into one aggregate in 11 μs and 3 μs for the Gem-based and Ptx-based polymer prodrugs, respectively. Furthermore, their self-assembly process is associated to a continuous decrease of the system free energy, indicating that the nanoparticle formation is a thermodynamics-driven spontaneous process (Figure S4b). The size of the aggregate was quantified by computing their radius of gyration (R_g) on parts of the trajectories where only one aggregate is observed (Figure S5). As expected, the longer the linker (*digly*-TEG > *digly* > *amide* ~ *propa*), the higher R_g of the corresponding polymer prodrug aggregates for both drugs. In addition, the R_g values of Ptx-based

aggregates were always higher than those of Gem-based aggregates regardless of the linker, probably due to the larger chemical structure of Ptx than Gem.

Supramolecular organization of polymer prodrug nanoparticles

To study the supramolecular organization of the polymer prodrug nanoparticles, the trajectory parts of one self-assembled aggregate were analyzed. The radial distribution function (RDF) of each polymer prodrug component (i.e., PI, Gem, Ptx, linker and SG1), relative to the nanoparticle COM are displayed in Figure 3. It can be seen that PI mainly occupies the core of the *digly*-TEG-PI nanoparticles regardless of the nature of the drug. Conversely, Gem was more distributed at the edge of the nanoparticles due to its hydrophilicity (LogP_{ow} ~ -0.9 calculated in CGMD), whereas Ptx was more buried in the nanoparticle core due to its high hydrophobicity (LogP_{ow} ~ 6.3). Nevertheless, it could be noted that several hydroxyl, carbonyl and ester groups in Ptx can interact favorably with water, preventing them to be fully buried in the nanoparticles. We calculated that 10–30% of Ptx molecular surface remains accessible to the solvent in the aggregates, making them partly visible on the surface of the nanoparticles (Figure 3). Regarding the SG1 moiety, it is mainly observed at the periphery of Gem-based polymer prodrug nanoparticles, and rather slightly more buried in Ptx-based counterparts. With respect to the linker, its spatial distribution gets closer to the nanoparticle periphery as its hydrophilicity increases: *propa/amide* < *digly* < *digly*-TEG. This trend is more pronounced for Gem-based polymer prodrug nanoparticles than in their Ptx-based counterparts, because the strongly hydrophobic Ptx can drag the linker deeper into the nanoparticle core than Gem can. The location of the potential cleavage sites (ester and amide groups) of the linkers was also investigated. The ester group from diglycolate next to the ethylene glycol moiety (*site 2*) is always located more closely to the surface of the nanoparticles compared to the amide/propa group near the drug (*site 1*) and the ester group near the PI chain (*site 3*), regardless of the nature of the drug. In addition, *site 2* moves closer to the surface of the nanoparticles as its hydrophilicity increased, while *site 1* and *site 3* showed only slight perturbation (Figure S6).

Snapshots extracted from the simulation trajectories of polymer prodrug nanoparticles (Figure 3) revealed that drugs were inhomogeneously distributed on the surface of the nanoparticles. This was confirmed by the calculation of the drug pair correlation functions which exhibit a main peak at a distance equal to about twice the drug radius of gyration, indicating that the drugs are in contact with each other

(Figure S7). In comparison, the pair correlation functions between SG1 groups were mainly distributed at a distance around 3 times of their radius of gyration, indicating that they are separated from each other. It should be noted that the second minor peak obtained for the Gem pair correlation functions suggests a tight ordered packing of the Gem moieties. While a smaller pair correlation function was observed between Ptx groups, which were mainly distributed at a distance of about 2 times their radius of gyration, the narrow single peak indicates the more compact interaction between Ptx moieties due to the stronger hydrophobic interaction (Figure S7). Overall, our data indicate that changing the nature of the linker has a greater influence on their own location (especially the cleavage *site 2*) within the nanoparticles, rather than on the supramolecular organization of polymer prodrug nanoparticles and for instance on the location of the drugs.

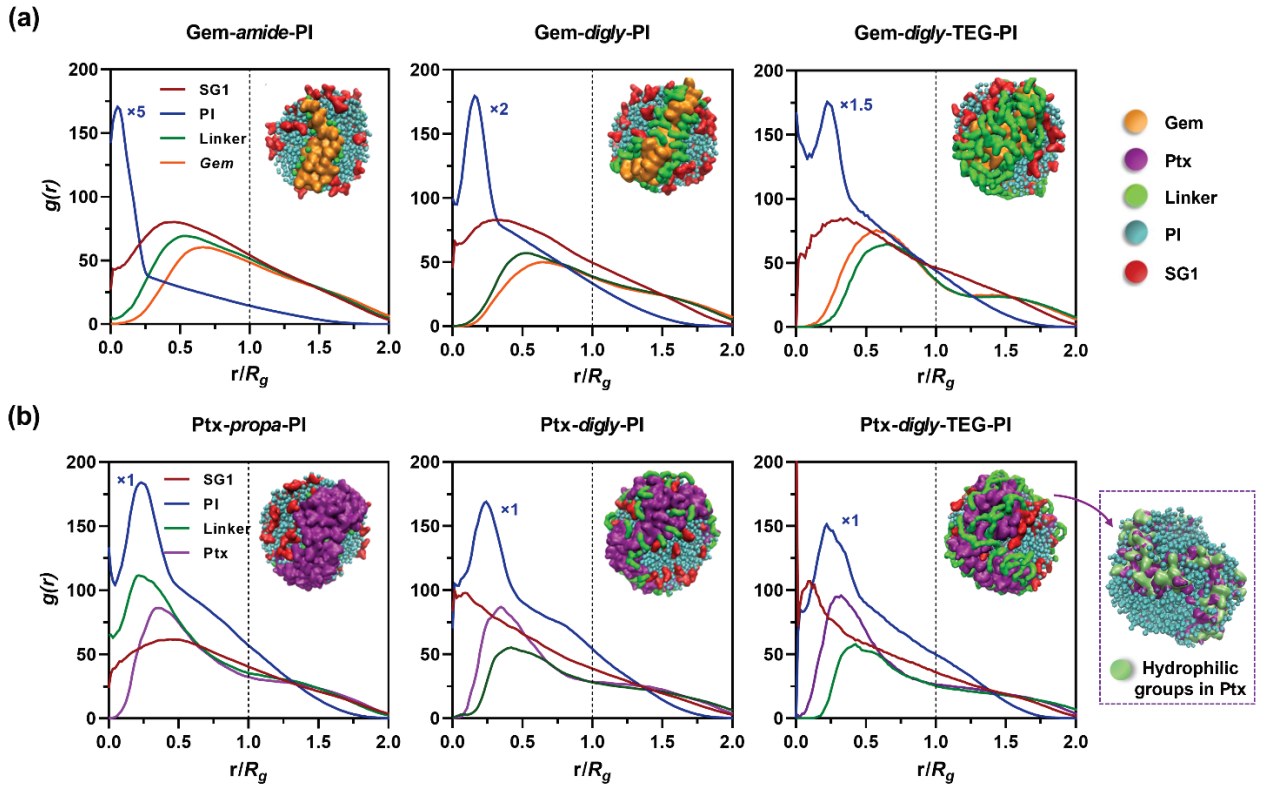

Figure 3. Radius distribution function of: (a) Gem-based and (b) Ptx-based polymer prodrug components relative to the center of mass of nanoparticles and their comparison between the polymer prodrugs with different linkers (the inner snapshots represent the corresponding nanoparticle supramolecular organization in coarse-grained model). For clarity purposes, the *g(r)* of PI was scaled down and must be multiplied by the factor indicated in each graph to obtain the real values.

Solvation and water-accessibility of the linkers

One of the critical factors in drug release from prodrug nanoparticles is the solvent-accessibility of the linkers (and in particular of the different cleavage sites, if any) which must be cleaved to release the drug. The Gem- and Ptx-based polymer prodrugs investigated in this work contain several cleavages sites (Figure 4a). Due to its higher hydrophilicity, the *digly*-TEG linker is distributed more on the surface of the nanoparticles than the *propa*/*amide* and *digly* linkers, which increases its water accessibility (Figures 3). Nevertheless, as illustrated from a snapshot of drug-*digly*-TEG-PI nanoparticles in water (Figure 4b), the three cleavage sites of the linker are not homogeneously solvated regardless the nature of drugs, which prompted us to further investigate their SASAs.

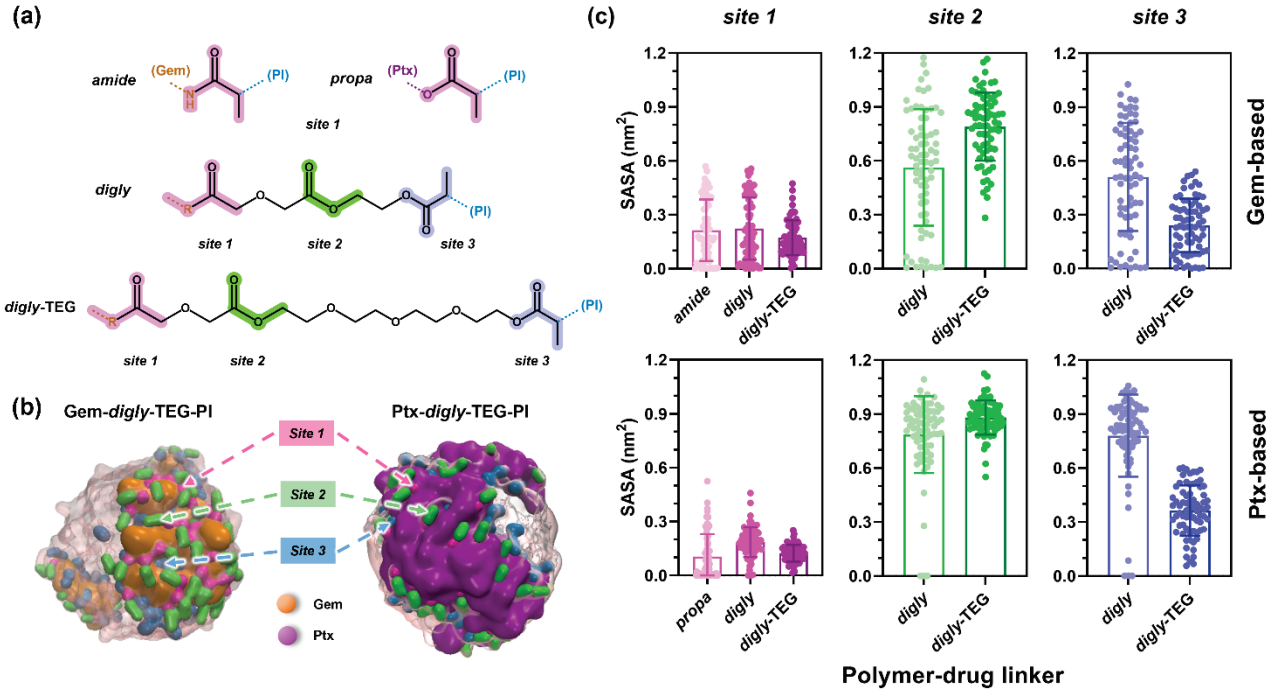

Figure 4. (a) Indication of the cleavage sites on the polymer prodrug chemical structures. (b) Location of the cleavage sites of the linkers shown on snapshots of Gem-*digly*-TEG-PI and Ptx-*digly*-TEG-PI nanoparticles in water (for the sake of clarity, PI and SG1 are made transparent). (c) Average and standard deviation of the solvent-accessible surface area (SASA) of each cleavage site of *propa*, *amide*, *digly* and *digly*-TEG linkers, in Gem-based (top row) and Ptx-based (bottom row) polymer prodrug nanoparticles (the solid dots indicate the SASA distribution per residues in polymer prodrugs, n = 72).

First, concerning the first cleavage site (*site 1*), an amide group sensitive to cathepsin B[61] for Gem and an ester group sensitive to esterases[62] for Ptx, it exhibits the lowest SASA values in both Gem-based and Ptx-based polymer prodrug nanoparticles (Figure 4c). Conversely, polymer prodrugs with linkers comprising multiple cleavage sites (i.e., *digly* and *digly*-TEG) present much higher SASA values. Interestingly, the SASA of the second cleavage site (*site 2*) of the *digly*-TEG linker is higher than that of the *digly* linker, both for Gem-based and Ptx-based polymer prodrug nanoparticles. The opposite tendency is observed for the third cleavage sites (*site 3*), probably because of the proximity of the hydrophobic PI chains which move them more inside the nanoparticles than for *site 2*. Note that *site 3* may result in poor drug release irrespectively of its location within the nanoparticles (Figure S6), because of its high steric hindrance[63]. Taken together, our data suggest that *site 2* would be the preferred cleavage site and that polymer prodrugs based on the longer, more hydrophilic *digly*-TEG linker could lead, as hypothesized, to improved drug release and thus cytotoxicity than those based on *digly* or *propa*/*amide* linkers. Note that cleavage of *site 2* yields a drug-*digly* moiety whose release from the nanoparticle will facilitate cleavage of *site 1* and release of the parent drug.

Free energy calculation for the release of drug-*digly* moieties from the nanoparticles

Although cleavage of the linker is a key step, this parameter alone is not sufficient to fully describe drug release from polymer prodrug nanoparticles. To this end, we performed Umbrella Sampling simulations to account for drug interactions with the different nanoparticle components and solvent molecules. The free energy of the drug-*digly* (resulting from cleavage of *site 2*) unbinding process was computed to gain insight into the drug release kinetics of Gem and Ptx. As shown in Figure 5, the free energy cost for Ptx-*digly* release from the nanoparticle (ΔG = 17.0 ± 0.01 kcal.mol^{-1}) is significantly higher than that of Gem-*digly* (ΔG = 6.8 ± 0.01 kcal.mol^{-1}), indicating that efficiency of Ptx-*digly* release would be much lower than for Gem-*digly*.

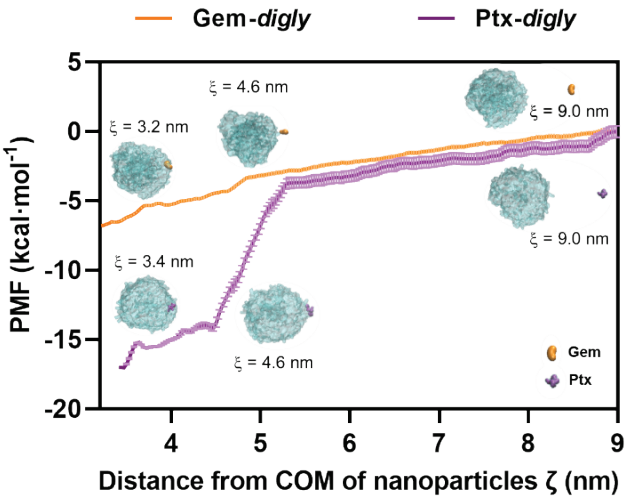

Figure 5. Free-energy profile, also called potential of mean force (PMF), of the release of Gem-*digly* (orange) and Ptx-*digly* (purple) from the corresponding polymer prodrug nanoparticles as a function of the distance from the COM of nanoparticles. The inner figures are snapshots of the drug release process at three different distances ($\xi = R_g$, 4.6 and 9.0 nm, respectively) in Gem-based and Ptx-based polymer prodrug nanoparticles. The transparent cyan material indicates the nanoparticles for better observation of the location of drug. The statistical errors were estimated from 100 bootstraps.

Experimental validation of the coarse-grained model-assisted design of polymer prodrugs

Synthesis of polymer prodrugs

To validate our coarse-grained model-assisted design of optimized polymer prodrug nanoparticles, Gem-*digly*-TEG-PI and Ptx-*digly*-TEG-PI were synthesized for further evaluation. To experimentally evaluate the added value of the *digly*-TEG linker, Gem-*amide*-PI, Gem-*digly*-PI and Ptx-*digly*-PI were also synthesized for comparison (note that Ptx-*propa*-PI was not synthesized due to the lack of expected release from such a hindered ester linker[63]).

All the polymer prodrugs were obtained by growing PI by nitroxide-mediated radical polymerization (NMP) from the corresponding drug-*linker*-functionalized alkoxyamine based on the SG1 nitroxide (Figure 6). More specifically, Gem (or Ptx) was linked under amidation (or esterification) reaction conditions to: (i) AMA-SG1, to yield Gem-*amide*-PI; (ii) *digly*-AMA-SG1, to yield Gem-*digly*-PI (or Ptx-*digly*-PI) and (iii) *digly*-TEG-

AMA-SG1, to yield Gem-*digly*-TEG-PI (or Ptx-*digly*-TEG-PI). The different drug-functionalized alkoxyamines were successfully obtained and fully characterized by ^{1}H and ^{13}C NMR as well as mass spectrometry (see experimental part and Figures S2 and S3).

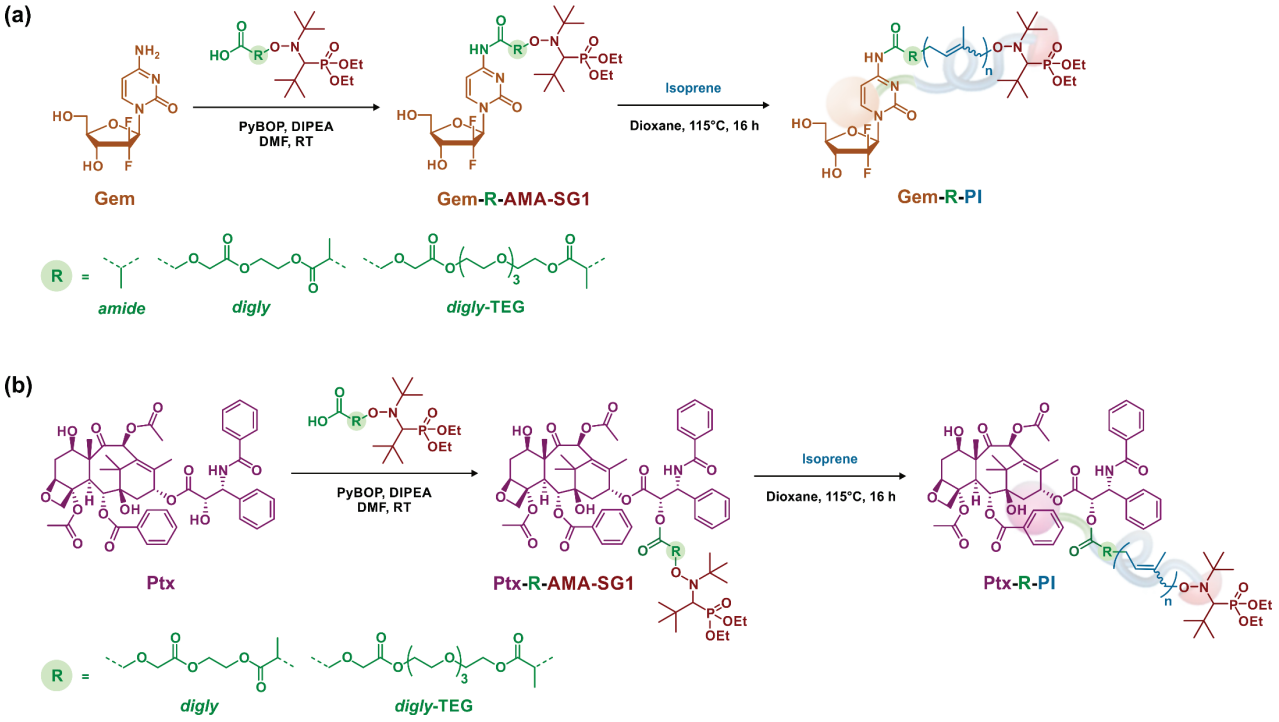

Figure 6. Chemical structures and synthesis strategies for Gem and Ptx-based alkoxyamine initiators and, their corresponding polymer prodrugs obtained by SG1-mediated nitroxide-mediated polymerization (NMP).

By using a $[isoprene]_0$:$[alkoxyamine]_0$ molar ratio of 200:1 to target small chain lengths and thus rather high drug loadings, well-defined Gem-based (M_n ~ 2.5–3.0 kg.mol^{-1}, $Đ$ = 1.12–1.21) and Ptx-based (M_n ~ 3.0 kg.mol^{-1}, $Đ$ = 1.07–1.14) polymer prodrugs were obtained (Table 2), as shown by SEC analyses (Figures 7a and 7b). The presence of the drugs at the extremity of the PI chains was confirmed by ^{1}H NMR spectroscopy based on the presence of proton signals characteristic of each drug; in particular the protons from the aromatic pyrimidine rings of Gem (δ =7.40-7.58 and 7.90–8.12 ppm) and the aromatic protons of Ptx (δ = 7.67-8.22) (Figures 7c and 7d). These proton signals were also used to determine the M_n of the polymer prodrugs by comparing them to those of PI repeat units (Table 2), resulting in pretty good agreement between $M_{n,SEC}$ and $M_{n,NMR}$ values. The drug loading was about 9-11 wt % for Gem-based polymer prodrugs, and

about 28-29 wt % for Ptx-based polymer prodrugs (Table 2). A drug free PI of similar M_n was also synthesized as a control by using the AMA-SG1 alkoxyamine under identical experimental conditions (Table 2).

Table 2. Macromolecular properties of Gem- and Ptx-based PI prodrugs, and colloidal properties of the corresponding nanoparticles.

Polymer prodrug	Conversion (%)	$M_{n,SEC}$[a] (g·mol^{-1})	$Đ$[a]	$M_{n,NMR}$ (g·mol^{-1})	D_z[e] (nm)	PDI[e]	ζ[f] (mV)	Drug loading[g] (wt %)
Gem-*amide*-PI	18	3010	1.21	3350[b]	173	0.09	-30.0	8.8
Gem-*digly*-PI	14	2490	1.13	4020[b]	168	0.01	-34.2	10.5
Gem-*digly*-TEG-PI	16	2500	1.12	3160[b]	189	0.07	-44.2	10.5
Ptx-*digly*-PI	13	2980	1.11	3126[c]	211	0.10	-36.1	28.7
Ptx-*digly*-TEG-PI	17	3040	1.07	3675[c]	169	0.07	-32.8	28.1
PI	31	2320	1.14	1866[d]	190	0.10	-40.0	–

[a] Determined by SEC, calibrated with PS standards and converted into PI using Mark-Houwink-Sakurada parameters. [b] Calculated from ratio of areas under the peak at 7.40-7.58 and 7.90–8.12 ppm (aromatic pyrimidine H from Gem) and 5.0–5.5 ppm (vinylic H in isoprene repeat unit (1,4-addition), corresponding to 81.2% of total isoprene unit[36]), according to $M_{n,NMR} = MW_{alkoxyamine} + DP_{n,NMR} \times MW_{isoprene}$. [c] Calculated from ratio of areas under the peak at 7.67–8.22 ppm (aromatic H from Ptx) over 5.0–5.5 ppm (vinylic H in isoprene repeat unit (1,4-addition), corresponding to 81.2% of total isoprene units), according to $M_{n,NMR} = MW_{alkoxyamine} + DP_{n,NMR} \times MW_{isoprene}$. [d] Calculated from ratio of areas under the peak at 3.1–3.3 ppm (α-H to P in SG1 moiety) over 5.0–5.5 ppm (vinylic H in isoprene repeat unit (1,4–addition), corresponding to 81.2% of total isoprene units), according to $M_{n,NMR} = MW_{alkoxyamine} + DP_{n,NMR} \times MW_{isoprene}$. [e] Determined by DLS. [f] Zeta potential. [g] %drug = $MW_{drug}/M_{n,SEC}$.

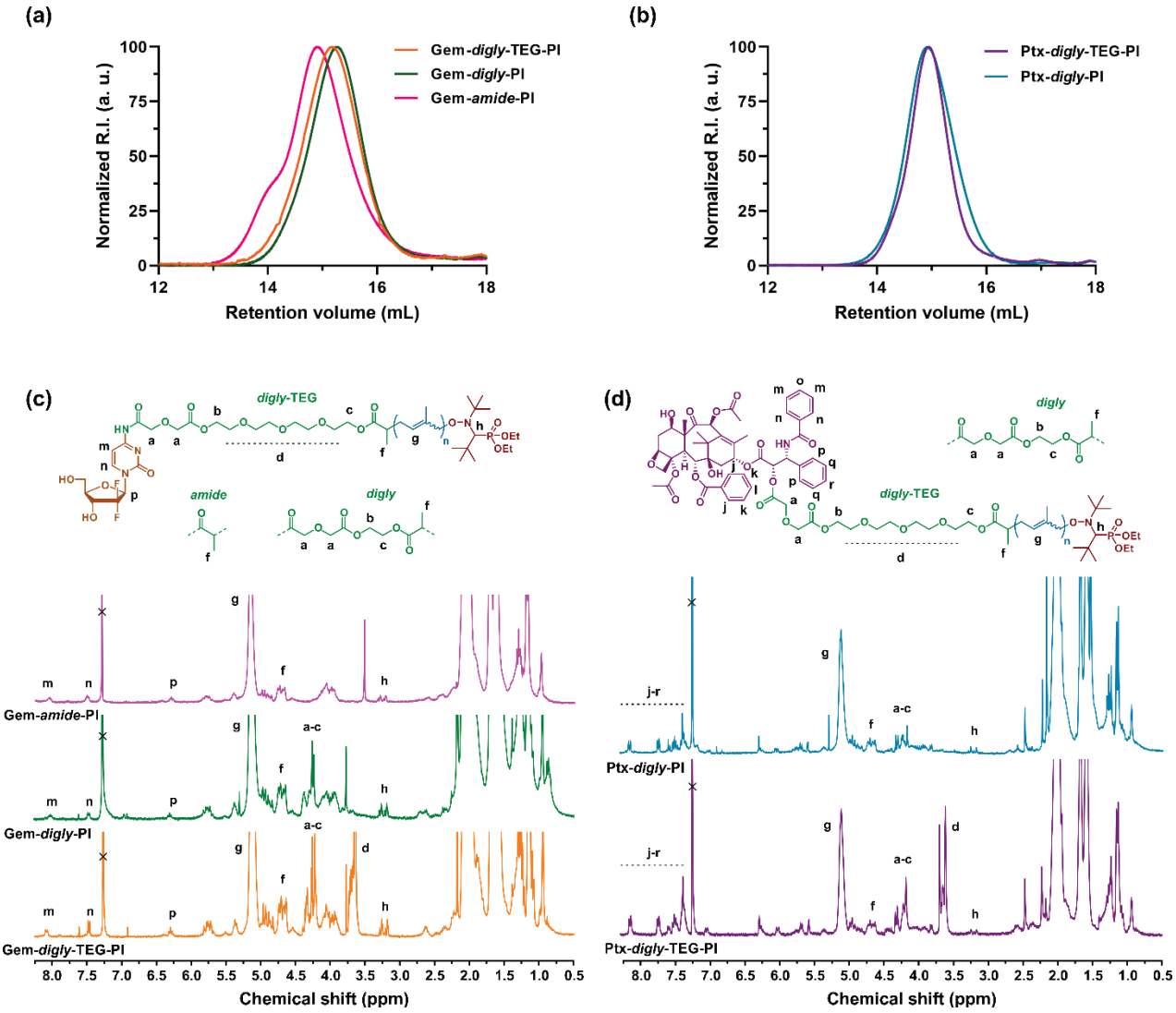

Figure 7. SEC chromatograms of: (a) Gem-based and (b) Ptx-based polymer prodrugs. ^{1}H NMR spectrum (300 MHz, $CDCl_3$) in the 0.5–8.5 ppm region of: (c) Gem-based and (d) Ptx-based polymer prodrugs.

Formulation of the polymer prodrug nanoparticles

Gem- and Ptx-based polymer prodrugs were then successfully formulated into surfactant-free nanoparticles by the nanoprecipitation technique[27] at a final concentration of 1.0 mg.mL^{-1}. The polymer prodrug nanoparticles exhibited average diameters in the 168–218 nm range with low polydispersity values (0.01–0.10), as measured by DLS (Table 2). Such controlled average diameter within ~50 nm is important to rule out potential influence of the nanoparticle size on their biological evaluation (e.g., drug release, cell uptake).

The morphology of polymer prodrug nanoparticles was characterized by cryo-TEM (Figures 8a and 8b) or TEM (Figure S8), which demonstrated spherical shapes with average diameters and narrow particle size distributions, in rather good agreement with DLS measurements. Interestingly, the spherical shape obtained experimentally for both types of drug is consistent with that obtained by coarse-grained simulation. The colloidal stability of the polymer prodrug nanoparticles was assessed by DLS, which showed constant average diameters and dispersities in water for at least 40 days (Figures 8c and 8d). Overall, these results also show that the new *digly*-TEG linker has no detrimental influence on the nanoparticle formation and on their colloidal properties.

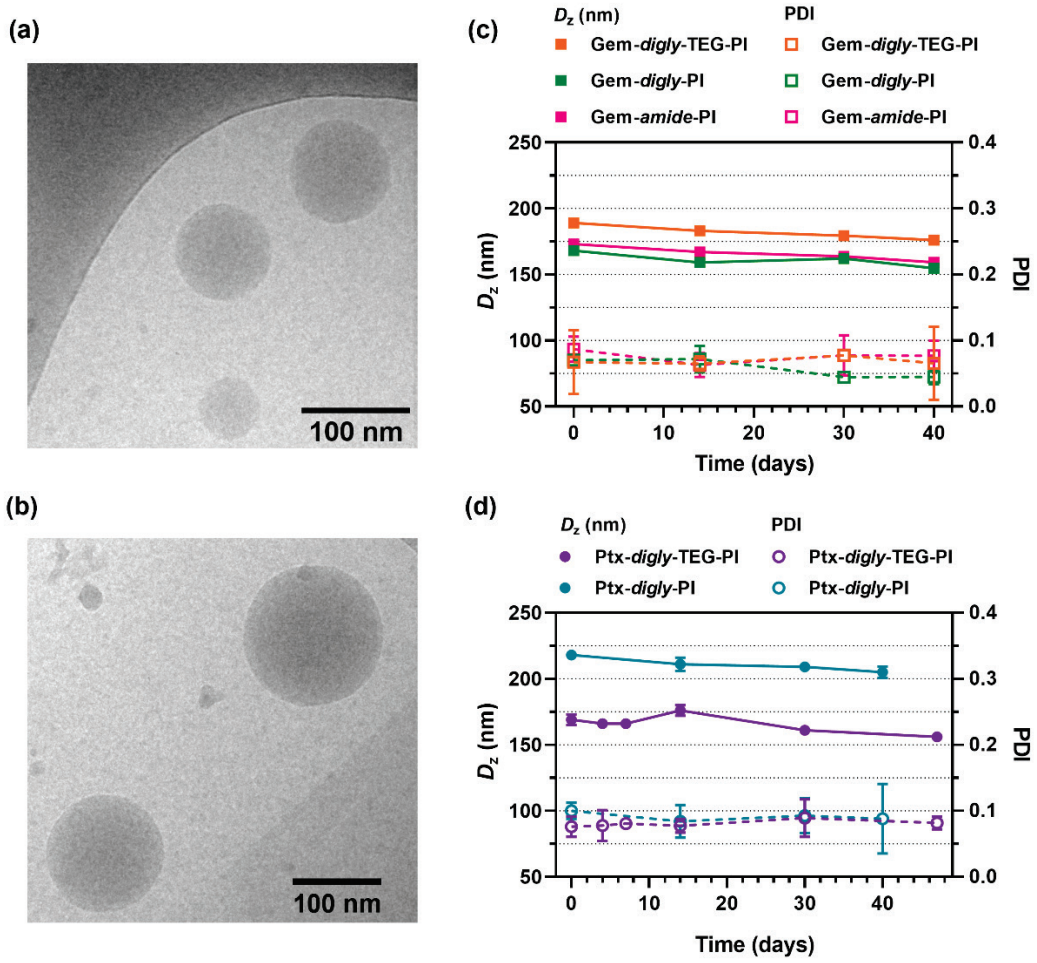

Figure 8. Representative Cryo-TEM images of Gem-*digly*-TEG-PI (a) and Ptx-*digly*-TEG-PI (b) polymer prodrug nanoparticles. Evolution with time of the intensity-average diameter (D_z) and the polydispersity index (PDI) of Gem-based (c) and Ptx-based (d) polymer prodrug nanoparticles.

Biological evaluations

Since coarse-grained simulations predicted higher solvent-accessible surface areas for the *digly*-TEG linker than for the *propa*/*amide* and *digly* linkers, Gem-*digly*-TEG-PI and Ptx-*digly*-TEG-PI polymer prodrug nanoparticles should lead to faster drug release (and thus greater cytotoxicity) than those made from the other linkers. To confirm this hypothesis, their drug release profile was monitored by HPLC at 37 °C in PBS and in human serum to mimic relevant biological environments. In PBS, Gem-*amide*-PI nanoparticles gave nearly no drug release (< 0.7 % after 48 h), whereas Gem-*digly*-PI and Gem-*digly*-TEG-PI nanoparticles exhibited ~4% and ~6% drug release, respectively, showing the beneficial effect of the *digly*-TEG linker (Figure 9a). The same effect was witnessed in human serum, in which Gem-*digly*-TEG-PI nanoparticles gave the highest drug release kinetics with ~19.5 % Gem released after 48 h, followed by Gem-*digly*-PI nanoparticles (~16 %) and Gem-*amide*-PI nanoparticles (1.1 %).

A similar trend was observed with Ptx-based polymer prodrug nanoparticles, as Ptx-*digly*-PI and Ptx-*digly*-TEG-PI nanoparticles gave very little Ptx release in PBS (~0.6 % after 48 h), whereas in human serum it reached 1.6 % and almost the double (3.0 %), respectively (Figure 9b). It should be noted that, according to the kinetic profile, a higher release of Ptx would certainly be achieved if the release was prolonged for a longer period.

These results first confirm the beneficial effect of using a *digly* moiety compared to an amide bond because of its higher hydrophilicity and an additional labile group (ester) in its structure, which does not require the presence of specific enzymes to amide groups (e.g., cathepsins) as it is the case for Gem-*amide*-PI nanoparticles. More importantly, the results also confirm for both drugs the supplementary beneficial effect of adding a TEG moiety, which improves solvation of the linker and promotes surface exposition and drug release also in human serum.

Interestingly, for a given medium (PBS or human serum), drug release from Gem-based polymer prodrug nanoparticles was always higher than that from Ptx-based polymer prodrug nanoparticles, although the SASA values of their cleavable *site 2* are similar (Figure 4c). This observation is in agreement with the drug-nanoparticle and drug-solvent interactions previously determined by coarse-grained simulation (Figure 5). Indeed, as indicated by the PMF profile of the drug unbinding process, higher energy is required to release Ptx-*digly* from nanoparticles in order to overcome the strong hydrophobic interactions between Ptx and the different nanoparticle components, compared to that required for Gem-*digly* (Figure 5).

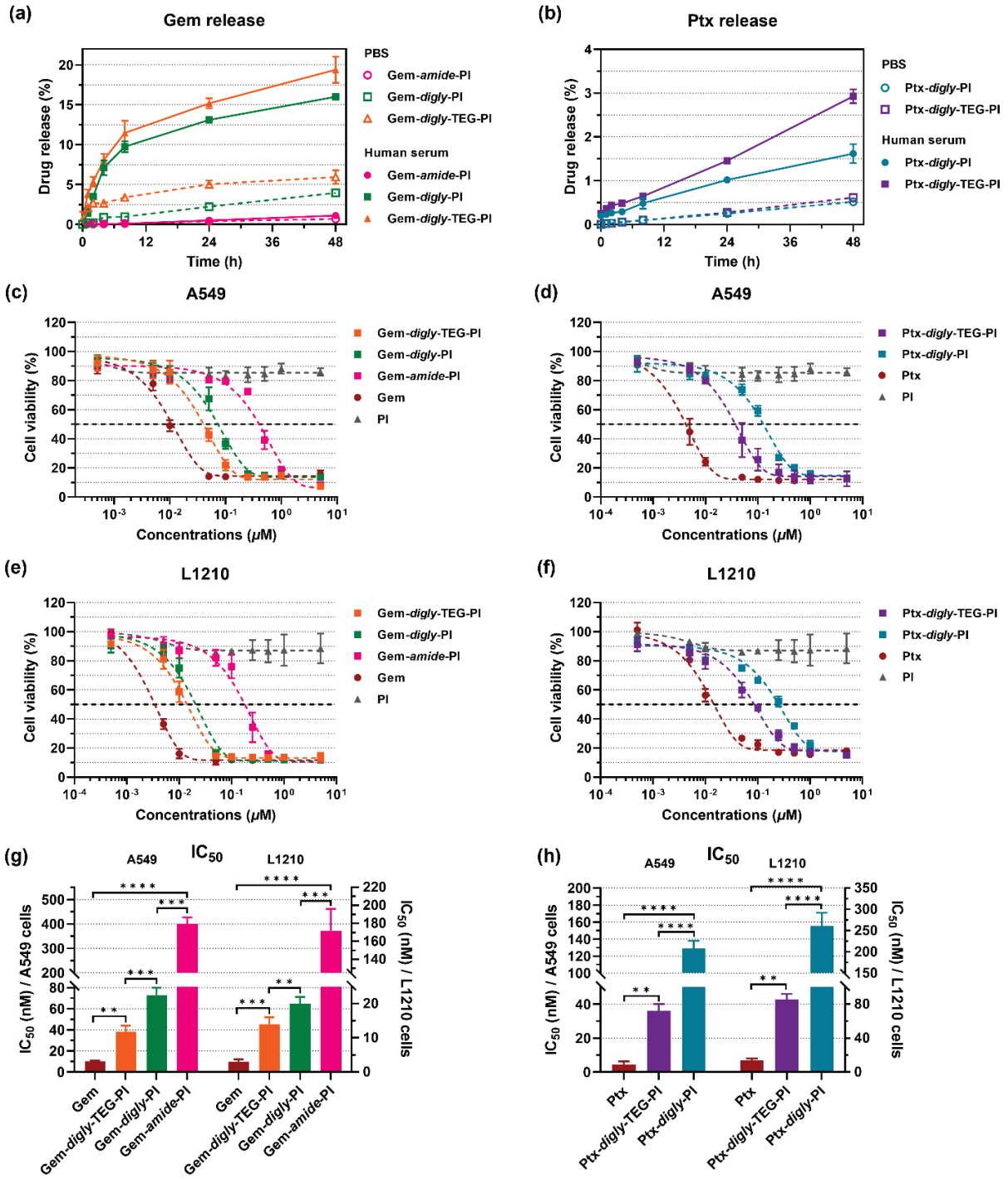

Figure 9. Drug release kinetics up to 48 h in PBS (open) or human serum (solid) at 37 °C obtained from: (a) Gem-*amide*-PI, Gem-*digly*-PI and Gem-*digly*-TEG-PI nanoparticles, and (b) Ptx-*digly*-PI and Ptx-*digly*-TEG-PI nanoparticles. Evolution of the cell viability (MTT test) of (c and d) A549 cells and (e and f) L1210 cells after incubation with increasing concentrations of (c and e) Gem-*amide*-PI, Gem-*digly*-PI and Gem-*digly*-TEG-PI nanoparticles and (d and f) Ptx-*digly*-PI and Ptx-*digly*-TEG-PI nanoparticles, as well as (g, h) the corresponding IC_{50} values. The values are expressed as the means ± SD. Unpaired two-tailed *t* test, ** $p < 0.01$, *** $p < 0.001$, **** $p < 0.0001$.

The *in vitro* cytotoxicity of the polymer prodrug nanoparticles was then evaluated by cell viability assay (MTT) on two relevant cancer cell lines: human lung cancer cells A549 and mouse leukemia cells L1210. Remarkably, as predicted by coarse-grained simulations, both Gem- and Ptx-based polymer prodrug nanoparticles showed increasing cytotoxicity with increasing linker hydrophilicity on both cell lines (Figures 9c–h). These results are also fully consistent with the release kinetics of Gem and Ptx (Figures 9a and 9b). Indeed, in both cell lines and for both drugs, polymer prodrug nanoparticles with the *digly*-TEG linker exhibited statistically lower IC_{50} values than those with the *digly* and *amide* linkers (in that order). On A549 cells, IC_{50} values of Gem-*amide*-PI, Gem-*digly*-PI and Gem-*digly*-TEG-PI nanoparticles were 400, 73 and 38 nM, respectively (Figures 9c and 9g), which is approaching the IC_{50} of free Gem (10 nM). Similarly, Ptx-*digly*-PI and Ptx-*digly*-TEG-PI nanoparticles exhibited IC_{50} values of 129 and 36 nM, respectively (Figures 9d and 9h), while IC_{50} of free Ptx was 4 nM. The same trends were also observed on L1210 cells (Figures 9e–9h). Gem-*amide*-PI, Gem-*digly*-PI and Gem-*digly*-TEG-PI nanoparticles gave IC_{50} values of 172, 20 and 14 nM, respectively, again approaching that of the parent drug (3 nM). For Ptx-*digly*-PI and Ptx-*digly*-TEG-PI nanoparticles, IC_{50} values were 261 and 85 nM, respectively, with IC_{50} of free Ptx equal to 14 nM. While the free drugs were more cytotoxic than any of the polymer prodrugs (as expected due the time needed for the drugs to be released), we also showed that the drug-free polymer (PI) was not cytotoxic at all concentrations tested in A549 and L1210 cells (Figures 9c–f), thus ruling out potential cytotoxicity of the polymer itself and confirming its cytocompatibility.

Interestingly, the beneficial effect of the TEG moiety was more pronounced for Ptx-based prodrugs than for their Gem-based counterparts. This is probably due to the hydrophilic nature of Gem which tends to mitigate the benefits of the hydrophilic linker (even if still present) whereas Ptx, which is strongly hydrophobic, requires an external hydrophilic environment to lead to efficient drug release. In fact, this demonstrates the robustness and sensitivity of our coarse-grained model which can also predict small differences in cytotoxicity through accurate determination of the spatial distribution of linkers and calculation of their solvent accessible surface areas, which represents the determining factor.

Conclusion

In this work, we have developed a methodology based on CG simulations to guide the development of optimized linkers for anticancer polymer prodrug nanoparticles and accurately predict their cytotoxicity on cancer cells. Our coarse-grained model, using MARTINI force fields, has enabled us to accurately determine the supramolecular organization of polymeric drug nanoparticles and, of particular interest, the drug-polymer linkers. By relying on the calculation of the SASA values of the different cleavage sites of the linkers developed so far (i.e., *propa*, *amide* and *digly*), we were able to propose a new linker, *digly*-TEG, with increased hydrophilicity and surface exposure (local linker steric hindrance) according to our simulations. The hypothesis and prediction that increasing the SASA value of the linker would increase the drug release and the cytotoxicity were then experimentally validated by synthesizing the corresponding polymer prodrugs based on either Gem or Ptx, and by investigating their drug release kinetics in PBS or in human serum and their cytotoxicity on 2 different representative cancer cell lines. Importantly, the results showed that increasing the linker hydrophilicity (*propa*/*amide* < *digly* < *digly*-TEG) resulted in increased drug release and cytotoxicity, in perfect agreement with our simulations and hypothesis. This CG model-assisted design of polymer prodrug nanoparticles is robust and highly versatile as it has been validated on polymer prodrugs based on two different drugs, three different linkers and two cancer cell lines.

Importantly, due to the transferable building block philosophy of the MARTINI force fields, new linkers can be easily implemented in existing CG models as only their bonded parameters have to be defined. This greatly simplifies the mapping and CG model building procedures, and allows for accelerating the determination of optimized structures.

To the best of our knowledge, this work represents the first example of using SASA values from a CG model to experimentally predict drug release kinetics and optimize the cytotoxicity of polymer prodrug nanoparticles. It also provides solid evidence that CG simulation could be developed as an accurate and forward-looking tool to better understand the supramolecular organization of various types of drug delivery systems, predict their drug release efficiency and other properties in order to develop optimized systems in a reduced amount of time.

Acknowledgement

The authors thank Dr. Julie Mougin and Stéphanie Denis (Institut Galien Paris-Saclay) for technical assistance in (Cryo-)TEM and cell culture, respectively. The authors acknowledge the financial support from the China Scholarship Council (fellowship 20190835003). This work was supported by HPC resources from GENCI-IDRIS (grant A0070710968). The CNRS and University Paris-Saclay are also acknowledged for financial support.

References

1. Ninomiya M, Tanaka K, Tsuchida Y, Muto Y, Koketsu M, Watanabe K. Increased Bioavailability of Tricin−Amino Acid Derivatives via a Prodrug Approach. *J. Med. Chem.* **54**, 1529-1536 (2011).
2. Dhaneshwar S, Tewari K, Joshi S, Godbole D, Ghosh P. Diglyceride prodrug strategy for enhancing the bioavailability of norfloxacin. *Chem. Phys. Lipids* **164**, 307-313 (2011).
3. Li Y*, et al.* Improving the oral bioavailability of tapentadol via a carbamate prodrug approach: synthesis, bioactivation, and pharmacokinetics. *Drug Deliv. and Transl. Res.* **8**, 1335-1344 (2018).
4. Vig BS, Huttunen KM, Laine K, Rautio J. Amino acids as promoieties in prodrug design and development. *Adv. Drug Deliv. Rev* **65**, 1370-1385 (2013).
5. Müller CE. Prodrug Approaches for Enhancing the Bioavailability of Drugs with Low Solubility. *Chem. Biodivers* **6**, 2071-2083 (2009).
6. Ikeda Y, Hisano H, Nishikawa Y, Nagasaki Y. Targeting and Treatment of Tumor Hypoxia by Newly Designed Prodrug Possessing High Permeability in Solid Tumors. *Mol. Pharmaceutics* **13**, 2283-2289 (2016).
7. Amitay Y*, et al.* Pharmacologic Studies of a Prodrug of Mitomycin C in Pegylated Liposomes (Promitil®): High Stability in Plasma and Rapid Thiolytic Prodrug Activation in Tissues. *Pharm Res* **33**, 686-700 (2016).
8. Mayr J*, et al.* An albumin-based tumor-targeted oxaliplatin prodrug with distinctly improved anticancer activity in vivo. *Chem. Sci.* **8**, 2241-2250 (2017).
9. Han H-K, Amidon GL. Targeted prodrug design to optimize drug delivery. *AAPS PharmSci* **2**, 48-58 (2000).
10. Mahato R, Tai W, Cheng K. Prodrugs for improving tumor targetability and efficiency. *Adv. Drug Deliv. Rev* **63**, 659-670 (2011).
11. Delplace V, Couvreur P, Nicolas J. Recent trends in the design of anticancer polymer prodrug nanocarriers. *Polym. Chem.* **5**, 1529-1544 (2014).
12. Duncan R. The dawning era of polymer therapeutics. *Nat Rev Drug Discov* **2**, 347-360 (2003).
13. Wei X*, et al.* Enzyme- and pH-Sensitive Branched Polymer–Doxorubicin Conjugate-Based Nanoscale Drug Delivery System for Cancer Therapy. *ACS Appl. Mater. Interfaces* **8**, 11765-11778 (2016).
14. Bordat A*, et al.* A Polymer Prodrug Strategy to Switch from Intravenous to Subcutaneous Cancer Therapy for Irritant/Vesicant Drugs. *J. Am. Chem. Soc.* **144**, 18844-18860 (2022).

15. Nguyen A, Böttger R, Li S-D. Recent trends in bioresponsive linker technologies of Prodrug-Based Self-Assembling nanomaterials. *Biomaterials* **275**, 120955 (2021).

16. Trung Bui D*, et al.* Polymer Prodrug Nanoparticles Based on Naturally Occurring Isoprenoid for Anticancer Therapy. *Biomacromolecules* **14**, 2837-2847 (2013).

17. Vinciguerra D*, et al.* Drug-Initiated Synthesis of Heterotelechelic Polymer Prodrug Nanoparticles for in Vivo Imaging and Cancer Cell Targeting. *Biomacromolecules* **20**, 2464-2476 (2019).

18. Zhuo S, Zhang F, Yu J, Zhang X, Yang G, Liu X. pH-Sensitive Biomaterials for Drug Delivery. *Molecules* **25**, 5649 (2020).

19. Tao Y, Liu S, Zhang Y, Chi Z, Xu J. A pH-responsive polymer based on dynamic imine bonds as a drug delivery material with pseudo target release behavior. *Polym. Chem.* **9**, 878-884 (2018).

20. Fu L, Sun C, Yan L. Galactose Targeted pH-Responsive Copolymer Conjugated with Near Infrared Fluorescence Probe for Imaging of Intelligent Drug Delivery. *ACS Appl. Mater. Interfaces* **7**, 2104-2115 (2015).

21. Jiang T, Li Y-M, Lv Y, Cheng Y-J, He F, Zhuo R-X. Amphiphilic polycarbonate conjugates of doxorubicin with pH-sensitive hydrazone linker for controlled release. *Colloids Surf. B: Biointerfaces* **111**, 542-548 (2013).

22. Ruan H, Hao S, Young P, Zhang H. Targeting Cathepsin B for Cancer Therapies. *Horiz Cancer Res* **56**, 23-40 (2015).

23. Li Y*, et al.* Cathepsin B-responsive nanodrug delivery systems for precise diagnosis and targeted therapy of malignant tumors. *Chin Chem Lett* **31**, 3027-3040 (2020).

24. Qiu N*, et al.* Esterase-Activated Charge-Reversal Polymer for Fibroblast-Exempt Cancer Gene Therapy. *Adv. Mater* **28**, 10613-10622 (2016).

25. Fukami T, Yokoi T. The emerging role of human esterases. *Drug Metab Pharmacokinet* **27**, 466-477 (2012).

26. Amissah F, Duverna R, Aguilar BJ, Poku RA, Kiros G-E, Lamango NS. Polyisoprenylated methylated protein methyl esterase overexpression and hyperactivity promotes lung cancer progression. *Am J Cancer Res* **4**, 116-134 (2014).

27. Martínez Rivas CJ*, et al.* Nanoprecipitation process: From encapsulation to drug delivery. *Int. J. Pharm* **532**, 66-81 (2017).

28. Frederix PWJM, Patmanidis I, Marrink SJ. Molecular simulations of self-assembling bio-inspired supramolecular systems and their connection to experiments. *Chem. Soc. Rev.* **47**, 3470-3489 (2018).

29. Singh N, Li W. Recent Advances in Coarse-Grained Models for Biomolecules and Their Applications. *Int. J. Mol. Sci* **20**, 3774 (2019).

30. Bochicchio D, Salvalaglio M, Pavan GM. Into the Dynamics of a Supramolecular Polymer at Submolecular Resolution. *Nat Commun* **8**, 147 (2017).

31. Weyandt E, Leanza L, Capelli R, Pavan GM, Vantomme G, Meijer EW. Controlling the length of porphyrin supramolecular polymers via coupled equilibria and dilution-induced supramolecular polymerization. *Nat Commun* **13**, 248 (2022).

32. Sarkar A*, et al.* Self-Sorted, Random, and Block Supramolecular Copolymers via Sequence Controlled, Multicomponent Self-Assembly. *J. Am. Chem. Soc.* **142**, 7606-7617 (2020).

33. Sasselli IR, Syrgiannis Z, Sather NA, Palmer LC, Stupp SI. Modeling Interactions within and between Peptide Amphiphile Supramolecular Filaments. *J. Phys. Chem. B* **126**, 650-659 (2022).

34. Rad-Malekshahi M*, et al.* The Supramolecular Organization of a Peptide-Based Nanocarrier at High Molecular Detail. *J. Am. Chem. Soc.* **137**, 7775-7784 (2015).

35. Gao P, Nicolas J, Ha-Duong T. Supramolecular Organization of Polymer Prodrug Nanoparticles Revealed by Coarse-Grained Simulations. *J. Am. Chem. Soc.* **143**, 17412-17423 (2021).

36. Harrisson S, Nicolas J, Maksimenko A, Bui DT, Mougin J, Couvreur P. Nanoparticles with In Vivo Anticancer Activity from Polymer Prodrug Amphiphiles Prepared by Living Radical Polymerization. *Angew. Chem. Int. Ed.* **52**, 1678-1682 (2013).

37. Bao Y, Guégain E, Mougin J, Nicolas J. Self-stabilized, hydrophobic or PEGylated paclitaxel polymer prodrug nanoparticles for cancer therapy. *Polym. Chem.* **9**, 687-698 (2018).

38. Pettersen EF*, et al.* UCSF Chimera—A visualization system for exploratory research and analysis. *J. Comput. Chem* **25**, 1605-1612 (2004).

39. Sousa da Silva AW, Vranken WF. ACPYPE - AnteChamber PYthon Parser interfacE. *BMC Res. Notes* **5**, 367 (2012).

40. Wang J, Wolf RM, Caldwell JW, Kollman PA, Case DA. Development and testing of a general amber force field. *J. Comput. Chem* **25**, 1157-1174 (2004).

41. Berendsen HJC, Postma JPM, van Gunsteren WF, DiNola A, Haak JR. Molecular dynamics with coupling to an external bath. *J. Chem. Phys.* **81**, 3684-3690 (1984).

42. Nosé S. A unified formulation of the constant temperature molecular dynamics methods. *J. Chem. Phys.* **81**, 511-519 (1984).

43. Hoover WG. Canonical dynamics: Equilibrium phase-space distributions. *Phys. Rev. A* **31**, 1695-1697 (1985).

44. Parrinello M, Rahman A. Polymorphic transitions in single crystals: A new molecular dynamics method. *J. Appl. Phys* **52**, 7182-7190 (1981).

45. Abraham MJ*, et al.* GROMACS: High performance molecular simulations through multi-level parallelism from laptops to supercomputers. *SoftwareX* **1**, 19-25 (2015).

46. Essmann U, Perera L, Berkowitz ML, Darden T, Lee H, Pedersen LG. A smooth particle mesh Ewald method. *J. Chem. Phys.* **103**, 8577-8593 (1995).

47. Hess B. P-LINCS: A Parallel Linear Constraint Solver for Molecular Simulation. *J. Chem. Theory Comput.* **4**, 116-122 (2008).

48. Marrink SJ, Risselada HJ, Yefimov S, Tieleman DP, de Vries AH. The MARTINI Force Field: Coarse Grained Model for Biomolecular Simulations. *J. Phys. Chem. B* **111**, 7812-7824 (2007).

49. Bussi G, Donadio D, Parrinello M. Canonical sampling through velocity rescaling. *J. Chem. Phys.* **126**, 014101 (2007).

50. Barker JA, Watts RO. Monte Carlo studies of the dielectric properties of water-like models. *Mol Phys* **26**, 789-792 (1973).

51. Torrie GM, Valleau JP. Nonphysical sampling distributions in Monte Carlo free-energy estimation: Umbrella sampling. *J. Comput. Phys* **23**, 187-199 (1977).

52. Kumar S, Rosenberg JM, Bouzida D, Swendsen RH, Kollman PA. THE weighted histogram analysis method for free-energy calculations on biomolecules. I. The method. *J. Comput. Chem* **13**, 1011-1021 (1992).

53. Cheng T*, et al.* Computation of Octanol−Water Partition Coefficients by Guiding an Additive Model with Knowledge. *J. Chem. Inf. Model.* **47**, 2140-2148 (2007).

54. Periole X, Knepp AM, Sakmar TP, Marrink SJ, Huber T. Structural Determinants of the Supramolecular Organization of G Protein-Coupled Receptors in Bilayers. *J. Am. Chem. Soc.* **134**, 10959-10965 (2012).

55. Hub JS, de Groot BL, van der Spoel D. g_wham—A Free Weighted Histogram Analysis Implementation Including Robust Error and Autocorrelation Estimates. *J. Chem. Theory Comput.* **6**, 3713-3720 (2010).

56. Bao Y*, et al.* Simple Synthesis of Cladribine-Based Anticancer Polymer Prodrug Nanoparticles with Tunable Drug Delivery Properties. *Chem. Mater.* **28**, 6266-6275 (2016).

57. Harrisson S, Couvreur P, Nicolas J. SG1 Nitroxide-Mediated Polymerization of Isoprene: Alkoxyamine Structure/Control Relationship and α,ω–Chain-End Functionalization. *Macromolecules* **44**, 9230-9238 (2011).

58. Harrisson S, Couvreur P, Nicolas J. Simple and efficient copper metal-mediated synthesis of alkoxyamine initiators. *Polym. Chem.* **2**, 1859-1865 (2011).

59. Vinciguerra D*, et al.* Heterotelechelic polymer prodrug nanoparticles: Adaptability to different drug combinations and influence of the dual functionalization on the cytotoxicity. *J. Controlled Release* **295**, 223-236 (2019).

60. Nicolas J. Drug-Initiated Synthesis of Polymer Prodrugs: Combining Simplicity and Efficacy in Drug Delivery. *Chem. Mater.* **28**, 1591-1606 (2016).

61. Dheer D, Nicolas J, Shankar R. Cathepsin-sensitive nanoscale drug delivery systems for cancer therapy and other diseases. *Adv. Drug Deliv. Rev* **151-152**, 130-151 (2019).

62. Di Consiglio E*, et al.* Human Variability in Carboxylesterases and carboxylesterase-related Uncertainty Factors for Chemical Risk Assessment. *Toxicol. Lett* **350**, 162-170 (2021).

63. Bao Y, Nicolas J. Structure–cytotoxicity relationship of drug-initiated polymer prodrug nanoparticles. *Polym. Chem.* **8**, 5174-5184 (2017).